SUPPORTING INFORMATION FOR PUBLICATION

Assembly of Heterometallic Rigid-Rod Complexes and Coordination Oligomers from Gold(I) Metalloligands

Verónica Cámara,[†] Natalia Barquero,[†] Delia Bautista,[‡] Juan Gil-Rubio,[,†] and José Vicente*[,†]*

[†]Grupo de Química Organometálica, Departamento de Química Inorgánica, Facultad de Química, Universidad de Murcia, E–30071 Murcia, Spain. [‡]SAI, Universidad de Murcia, E–30071 Murcia, Spain

Contents:

Figures S18-22. NMR spectra of $[Co(TpylC_6H_4C{\equiv}CAuPPh_3)_2](BF_4)$.

Figures S23-S27. NMR spectra of $[Fe(TpylC_6H_4C{\equiv}CAuCNXy)_2](ClO_4)_2$.

Figures S28-S33. NMR spectra of $[Zn(TpylC_6H_4C{\equiv}CAuCNXy)_2](TfO)_2$.

Figures S34-37. NMR spectra of $[Co(TpylC_6H_4C{\equiv}CAuCNXy)_2](BF_4)_2$.

Figure S38. ^1H NMR spectrum of $[Fe\{(TpylC_6H_4C{\equiv}C)_2Au\}]_n(ClO_4)_n$.

Figures S39 and 40. NMR spectra of $[Zn\{(TpylC_6H_4C{\equiv}C)_2Au\}]_n(ClO_4)_n$.

Figures S41 and 42. NMR spectra of $[Co\{(TpylC_6H_4C{\equiv}C)_2Au\}]_n(BF_4)_n$.

Figure S43. Representation of the crystal structure of $[Co(TpylC_6H_4C{\equiv}CAuPPh_3)_2](BF_4)_2{\cdot}(MeCN)_4$ showing the C–H···F–B interactions.

Table S1. C–H···F bond distances (Å) and angles (deg) of $[Co(TpylC_6H_4C{\equiv}CAuPPh_3)_2](BF_4)_2{\cdot}(MeCN)_4$.

Figure S44. Representation of the crystal structure of the cation $[Co(TpylC_6H_4C{\equiv}CAuPPh_3)_2]^{2+}$ showing significant longitudinal molecular dimensions.

Figure S45. SEC profiles of oligomers $[M\{(TpylC_6H_4C{\equiv}C)_2Au\}]_n(X)_n$.

Synthesis of $[Co(TpylC_6H_4C{\equiv}CH)_2](BF_4)_2$. This was prepared in the same way as the analogous heterometallic complexes, starting from $TpylC_6H_4C{\equiv}CH$ (165 mg, 0.50 mmol) and $Co(BF_4)_2{\cdot}6H_2O$ (84 mg, 0.25 mmol). An orange brown solid was obtained. Yield: 208 mg, 0.22 mmol, 90%. Mp: 284 °C (d). Anal. Calcd for $C_{46}H_{30}B_2CoF_8N_6{\cdot}(H_2O)_{1.5}$: C, 59.64; H, 3.59; N, 9.07. Found: C, 59.86; H, 3.55; N 8.89. IR (KBr) $\tilde{\nu}$ (cm^{-1}): 3259 (≡C–H), 2103 (C≡C), 1058 (B–F). ^{1}H NMR (400.9 MHz, CD_3CN): δ 91.86 (br s, 4H, H6), 53.48 (s, 4H, H3), 40.44 (s, 4H, H3'), 32.52 (s, 4H, H5), 13.49 (vd, J = 6.0 Hz, 4H, C_6H_4), 9.53 (s, 4H, H4), 9.08 (vd, J = 6.0 Hz, 4H, C_6H_4), 4.92 (s, 2H, HC≡C). $^{13}C\{^1H\}$ NMR (75.5 MHz, CD_3CN): δ 161.6, 153.8 (C4), 142.0 (CH, C_6H_4), 121.8 (C), 120.4 (CH, C_6H_4), 89.8 (*C*≡CH), 80.1 (C≡*C*H). Owing to the paramagnetic effect, 7 of the expected 14 signals were not observed. ^{19}F NMR (282.4 MHz, CD_3CN): : δ –150.41 (br s, $^{10}BF_4^-$), –150.46 (br s, $^{11}BF_4^-$). ESI-MS *m/z*: 812 ($[Co(TpylC_6H_4C{\equiv}CH)_2(BF_4)]^+$), 363 ($[Co(TpylC_6H_4C{\equiv}CH)_2]^{2+}$), 334 ($[HTpylC_6H_4C{\equiv}CH]^+$).

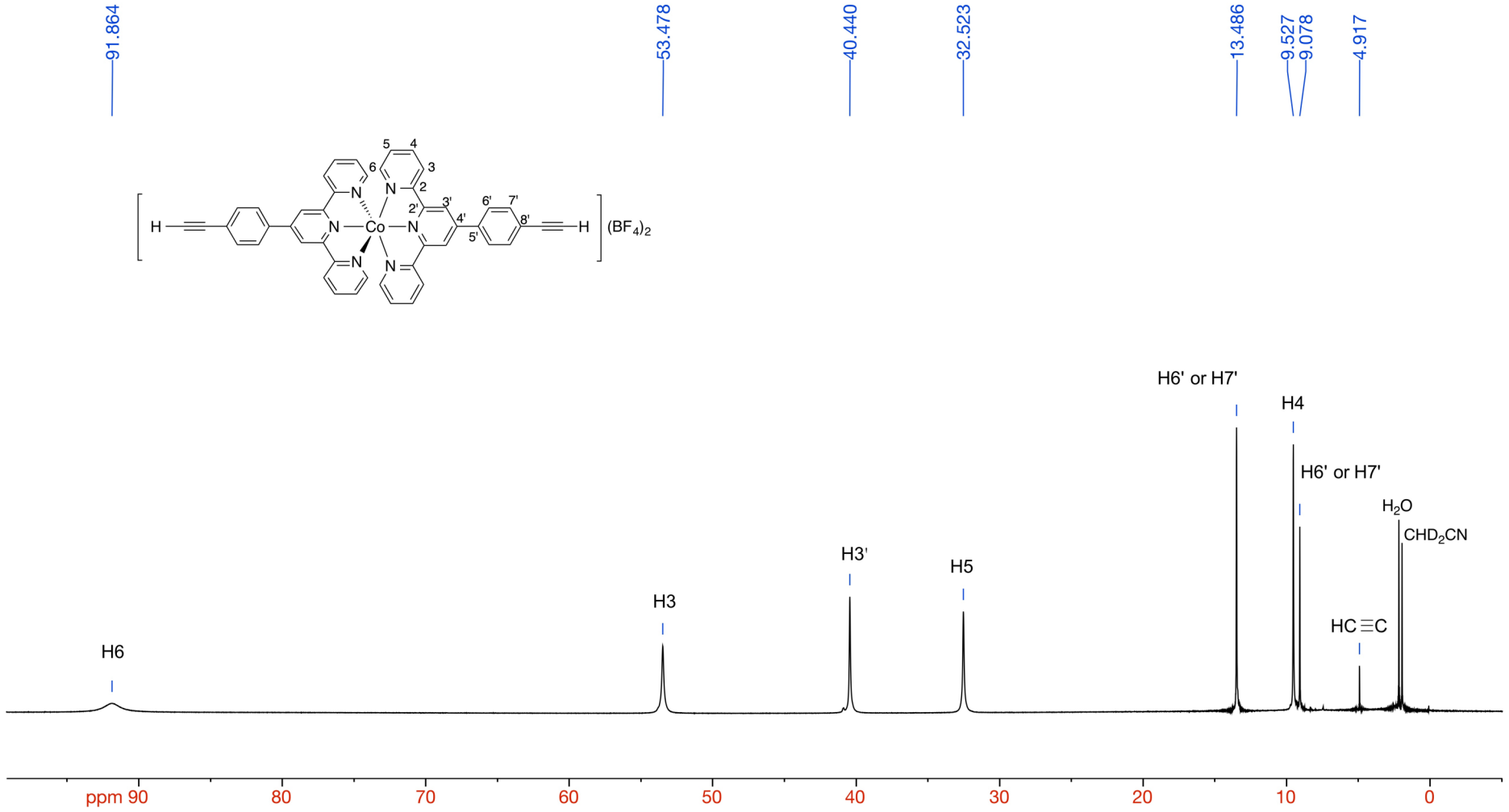

Figure S1. ^{1}H NMR (400.9 MHz, CD_3CN) spectrum of $[Co(TpylC_6H_4C{\equiv}CH)_2](BF_4)_2$.

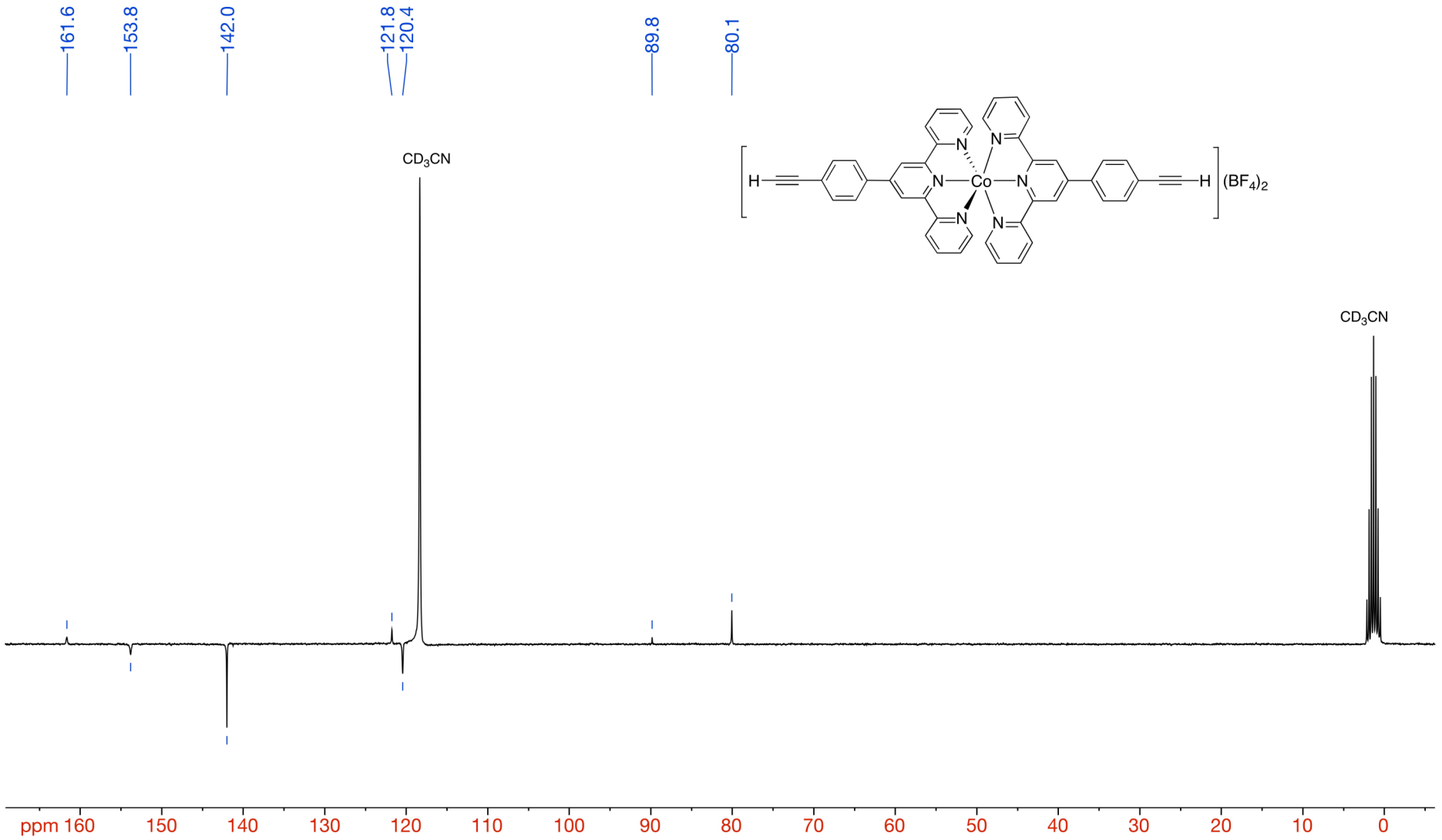

Figure S2. $^{13}C\{^{1}H\}$ NMR (75.5 MHz, CD_3CN) spectrum of $[Co(TpylC_6H_4C{\equiv}CH)_2](BF_4)_2$.

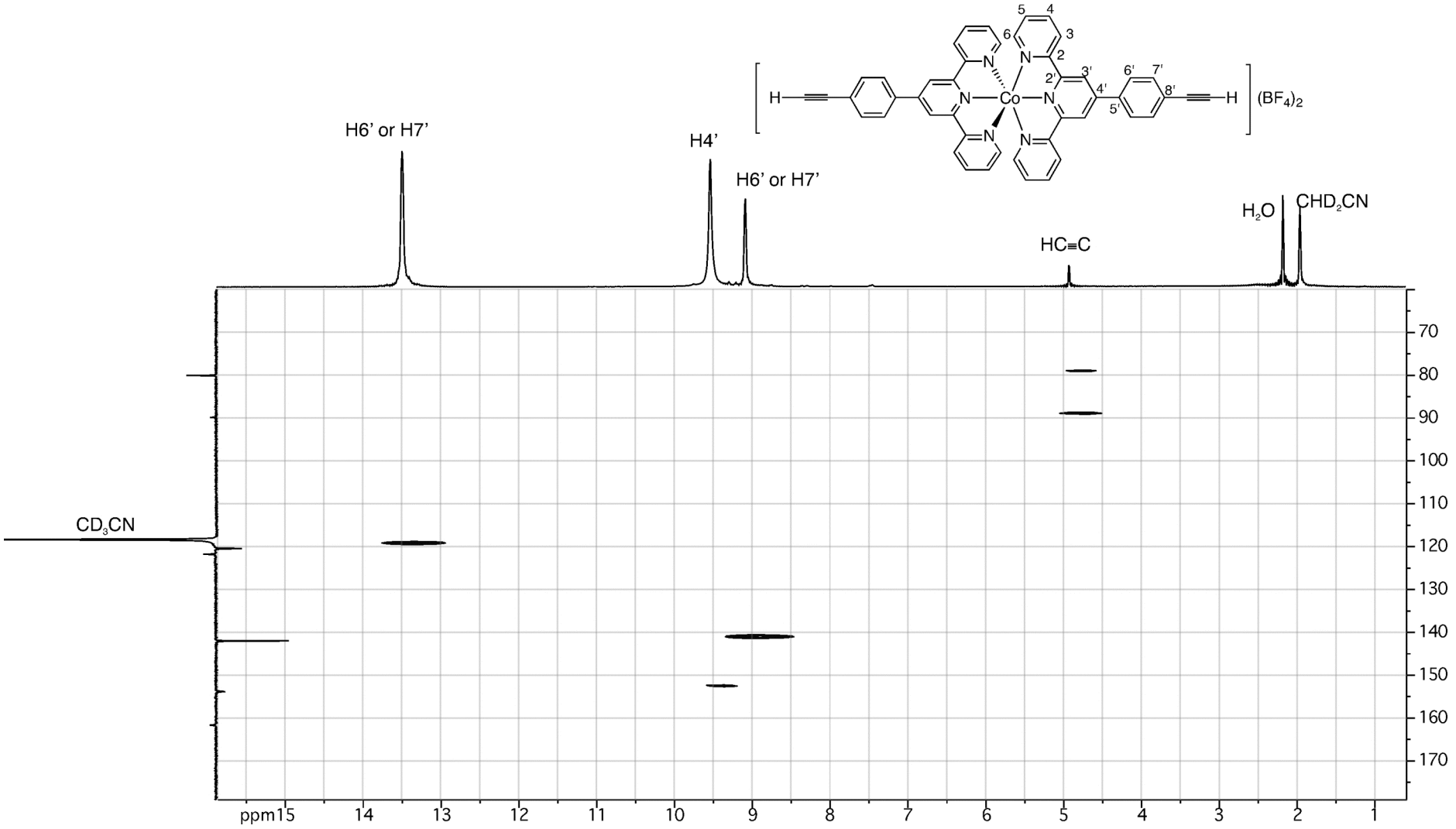

Figure S3. HMQC (300.1 MHz, CD_3CN) spectrum of $[Co(TpylC_6H_4C{\equiv}CH)_2](BF_4)_2$.

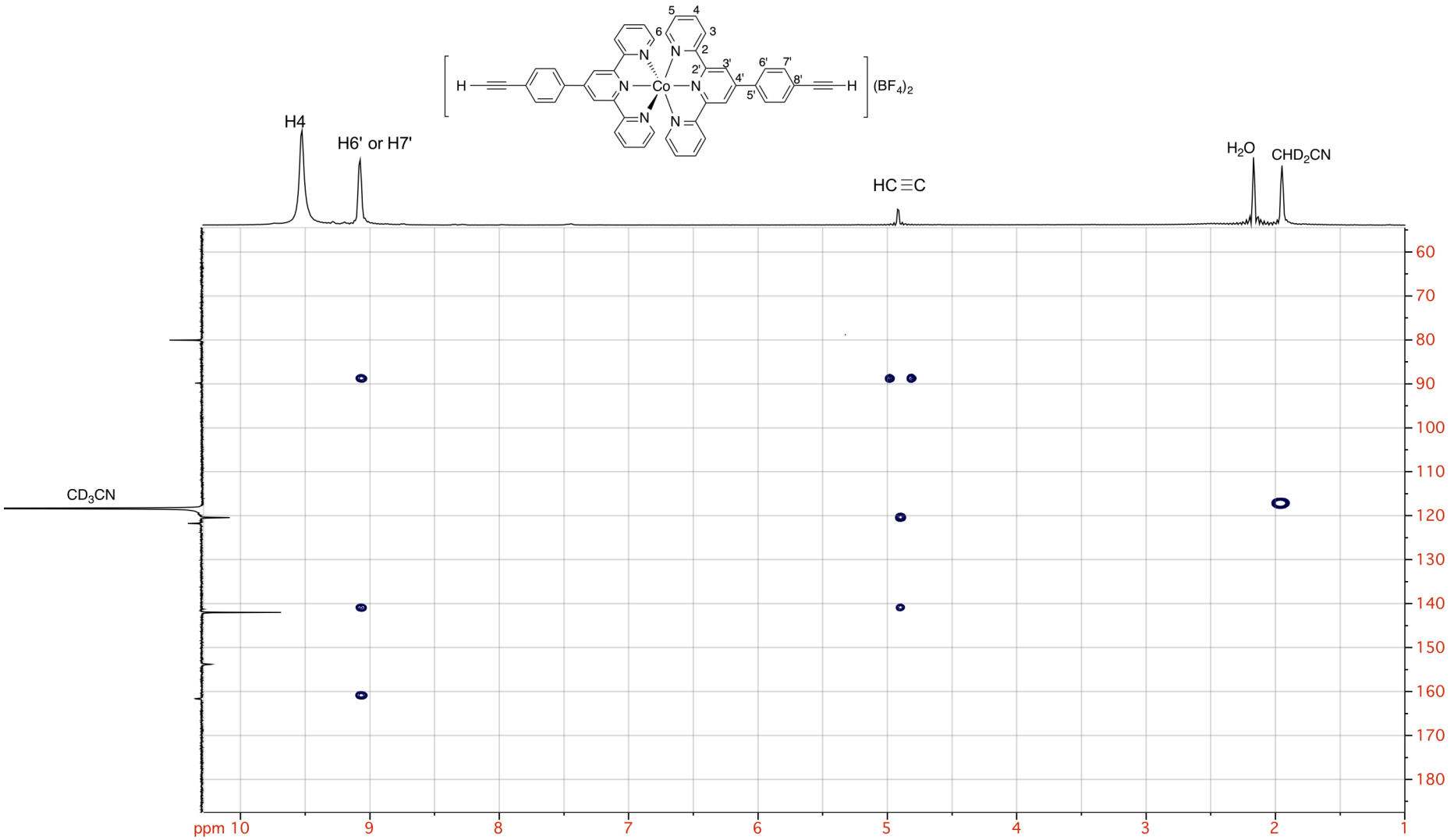

Figure S4. HMBC (300.1 MHz, CD_3CN) spectrum of $[Co(TpylC_6H_4C{\equiv}CH)_2](BF_4)_2$.

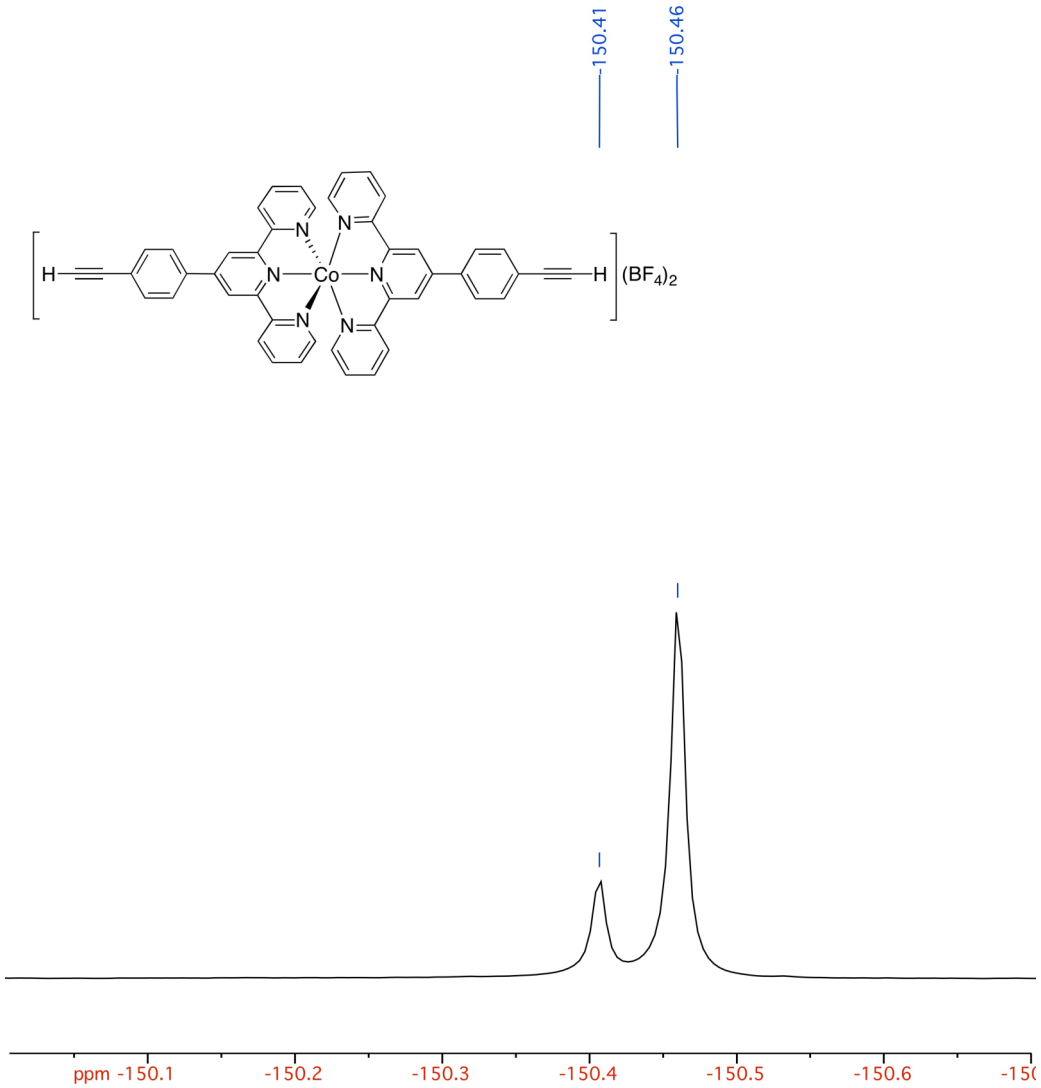

Figure S5. ^{19}F NMR (282.4 MHz, CD_3CN) spectrum of $[Co(TpylC_6H_4C{\equiv}CH)_2](BF_4)_2$.

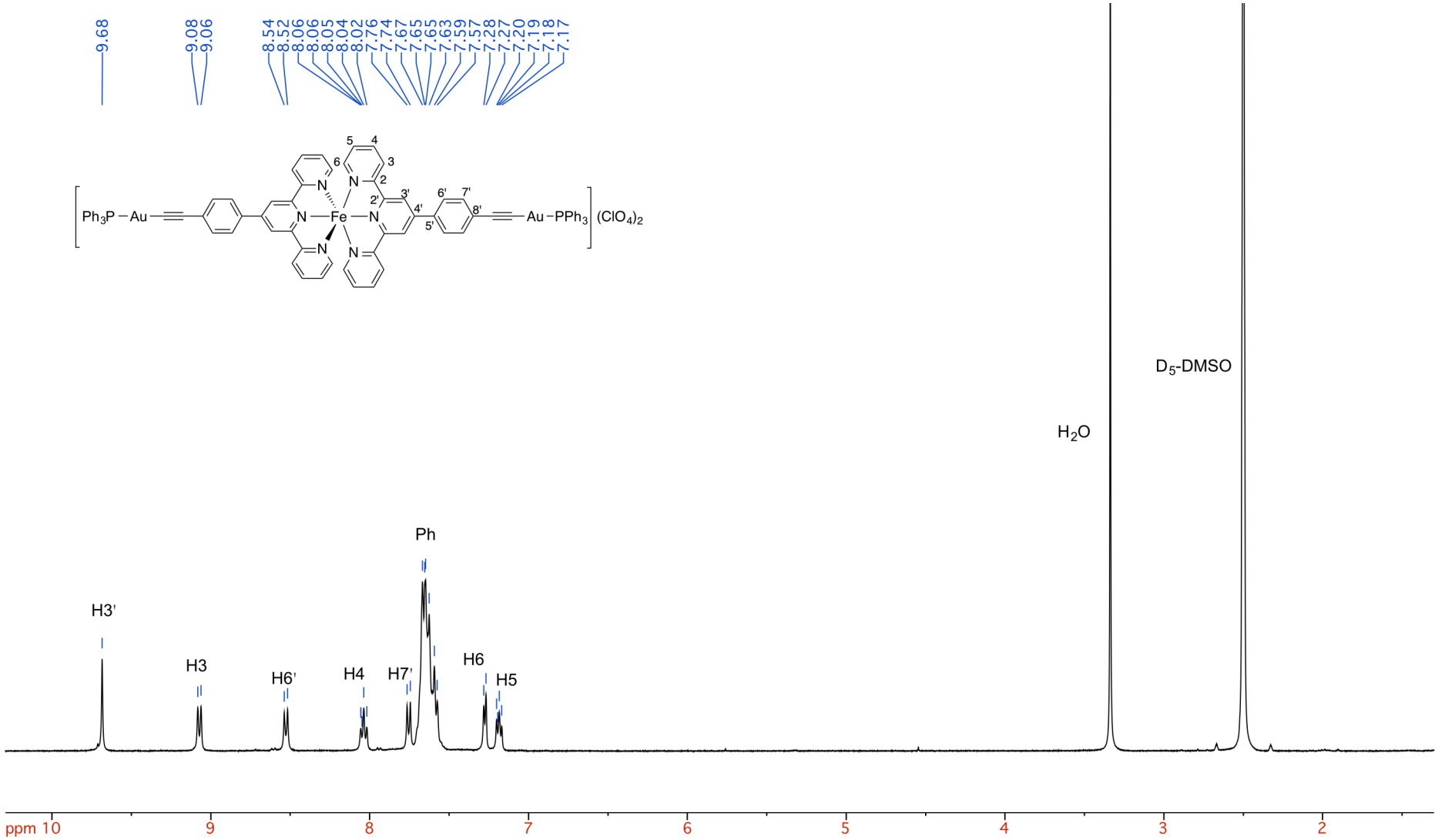

Figure S6. ^{1}H NMR (400.9 MHz, D_6-DMSO) spectrum of $[Fe(TpylC_6H_4C{\equiv}CAuPPh_3)_2](ClO_4)_2$.

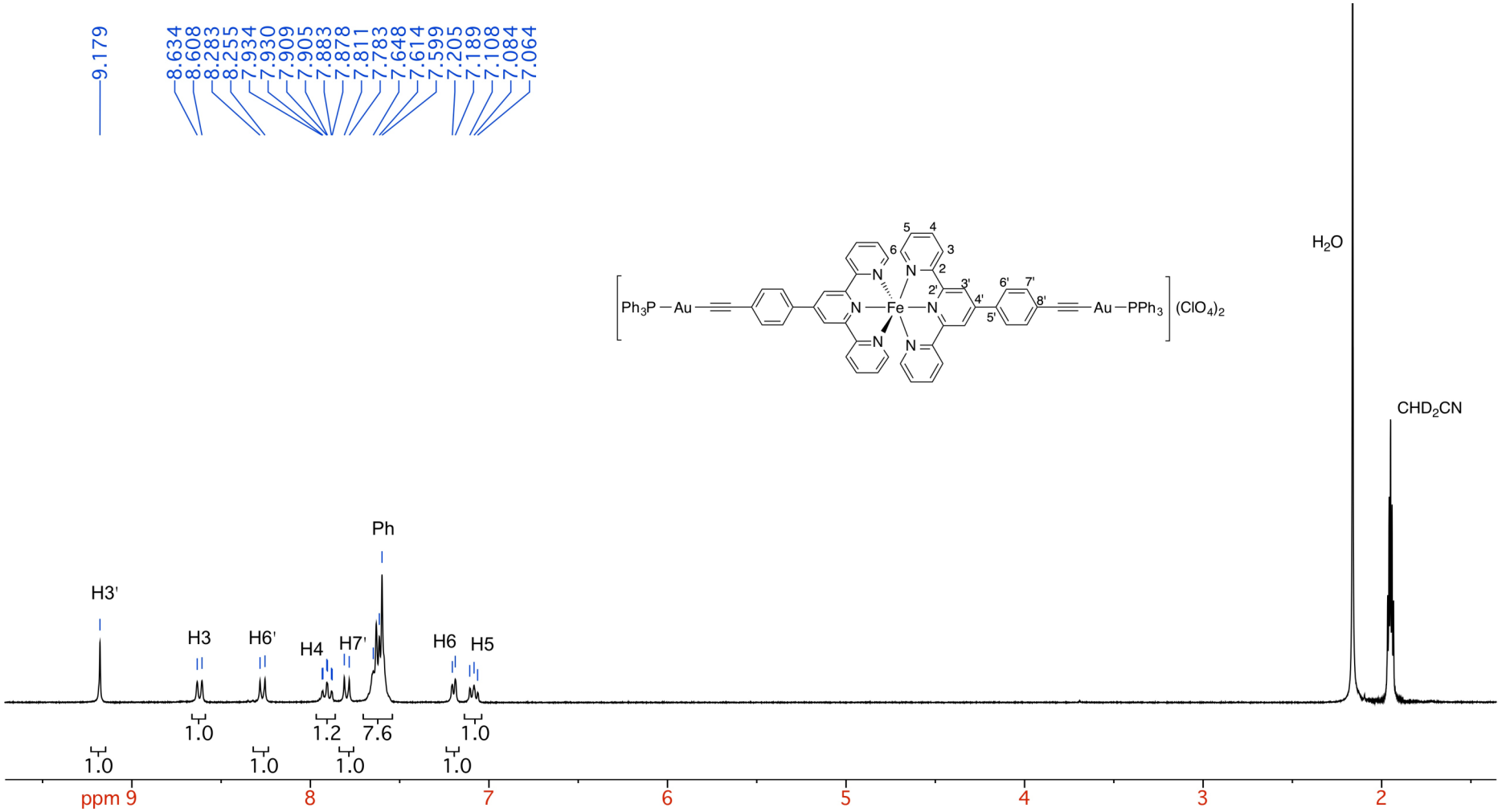

Figure S7. ^{1}H NMR (300.1 MHz, CD_3CN) spectrum of $[Fe(TpylC_6H_4C{\equiv}CAuPPh_3)_2](ClO_4)_2$.

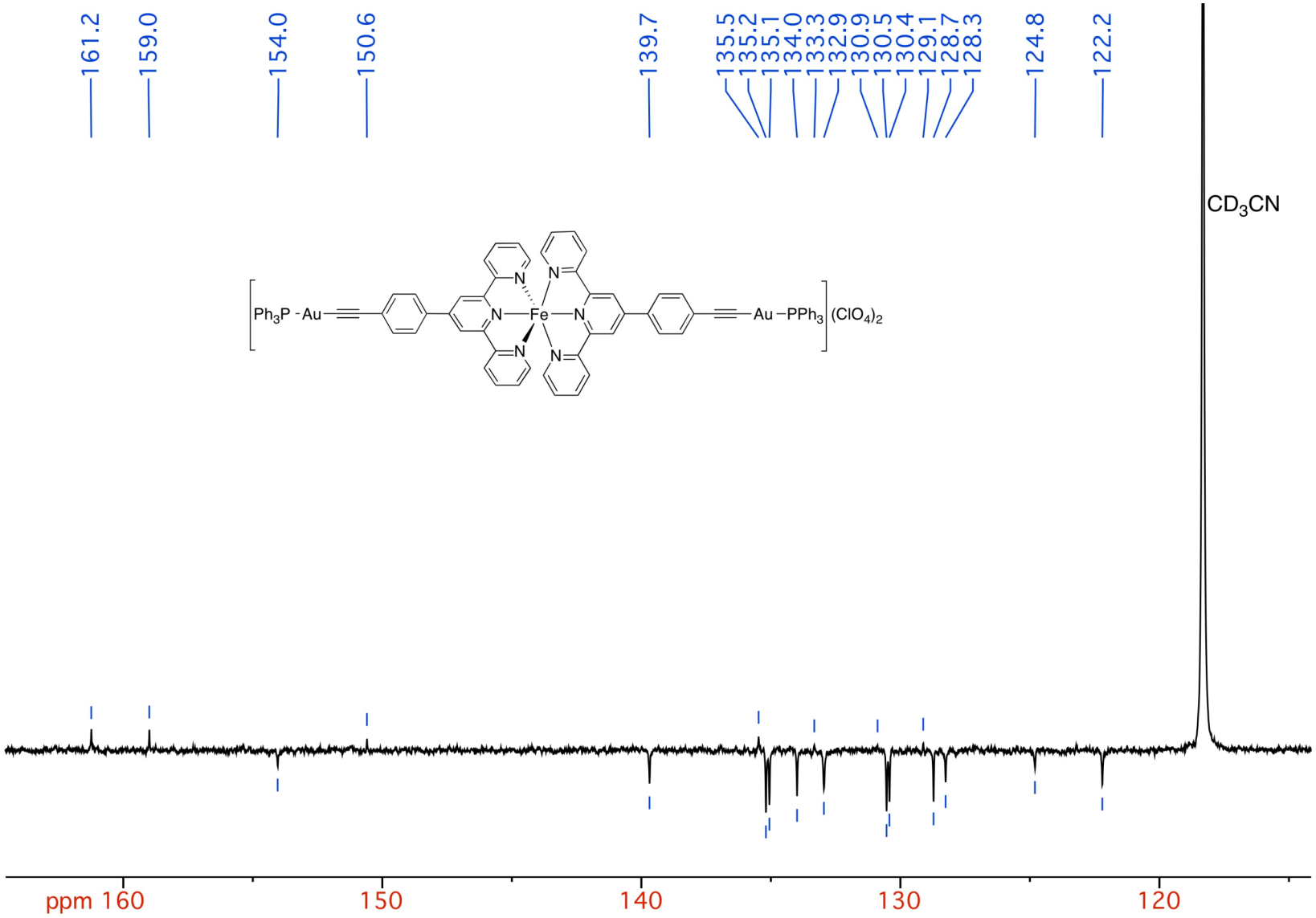

Figure S8. $^{13}C\{^{1}H\}$ NMR (100.8 MHz, CD_3CN) spectrum of $[Fe(TpylC_6H_4C{\equiv}CAuPPh_3)_2](ClO_4)_2$.

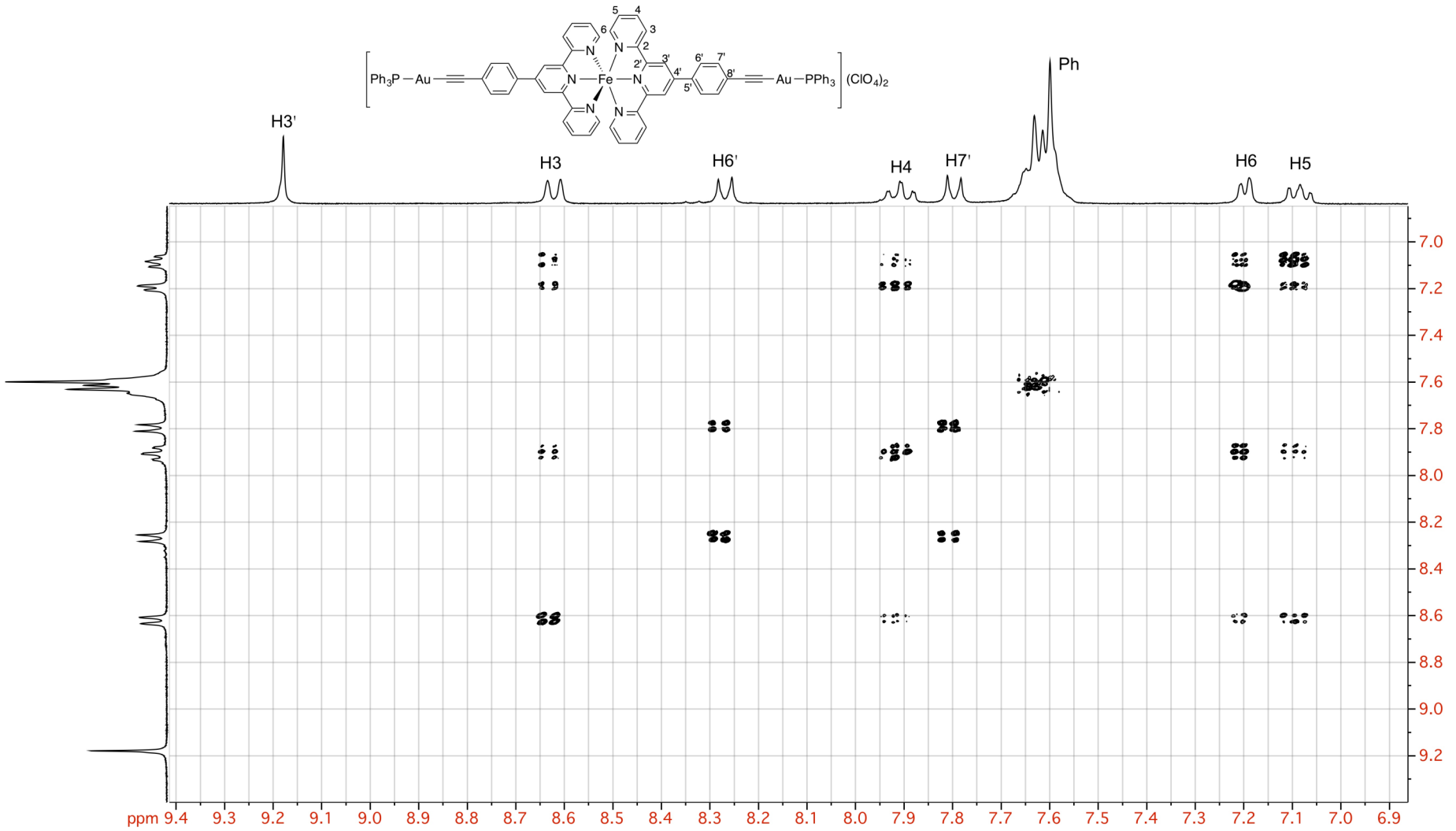

Figure S9. COSY (300.1 MHz, CD_3CN) spectrum of $[Fe(TpylC_6H_4C{\equiv}CAuPPh_3)_2](ClO_4)_2$.

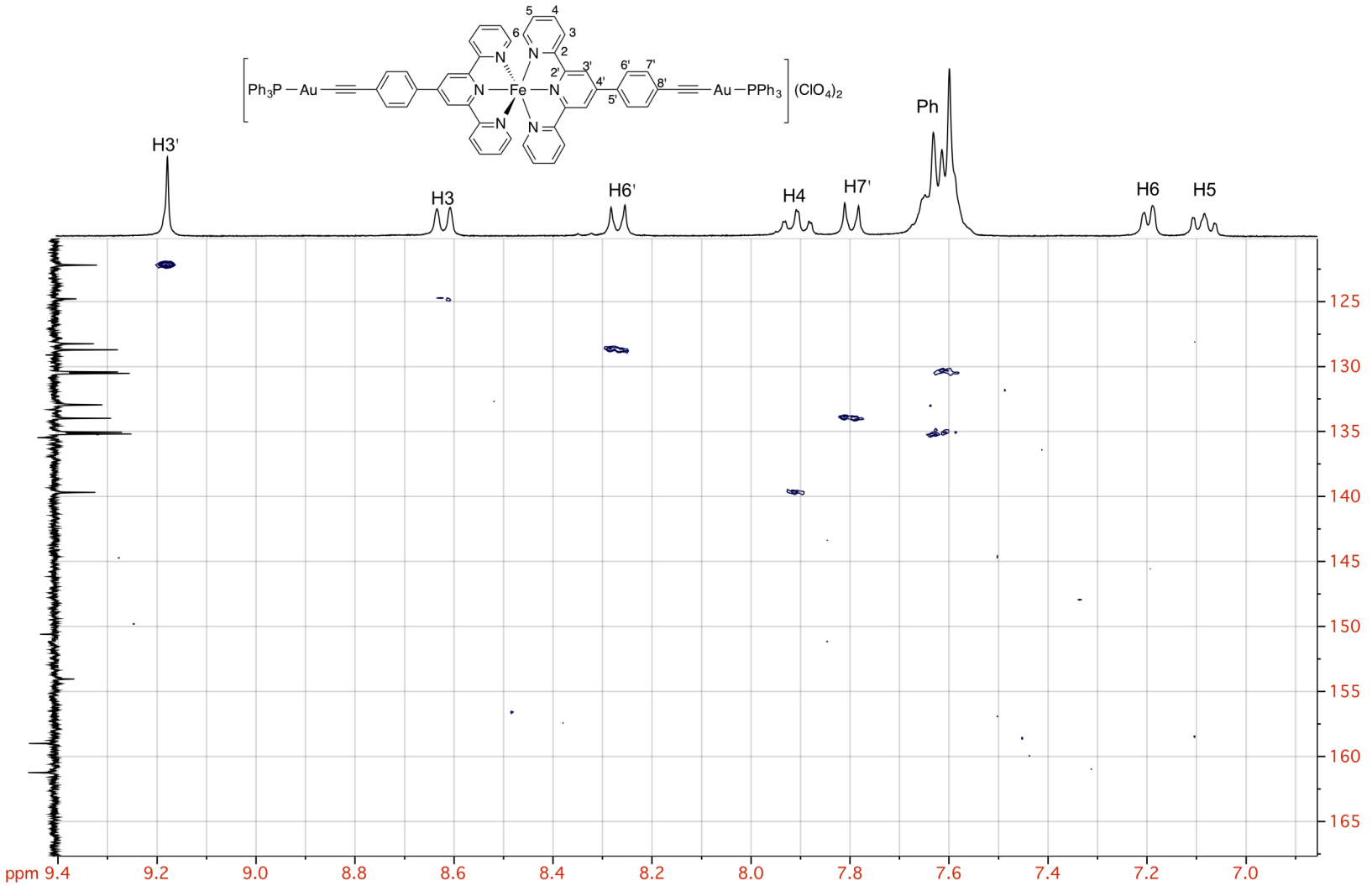

Figure S10. HMQC (300.1 MHz, CD_3CN) spectrum of $[Fe(TpylC_6H_4C{\equiv}CAuPPh_3)_2](ClO_4)_2$.

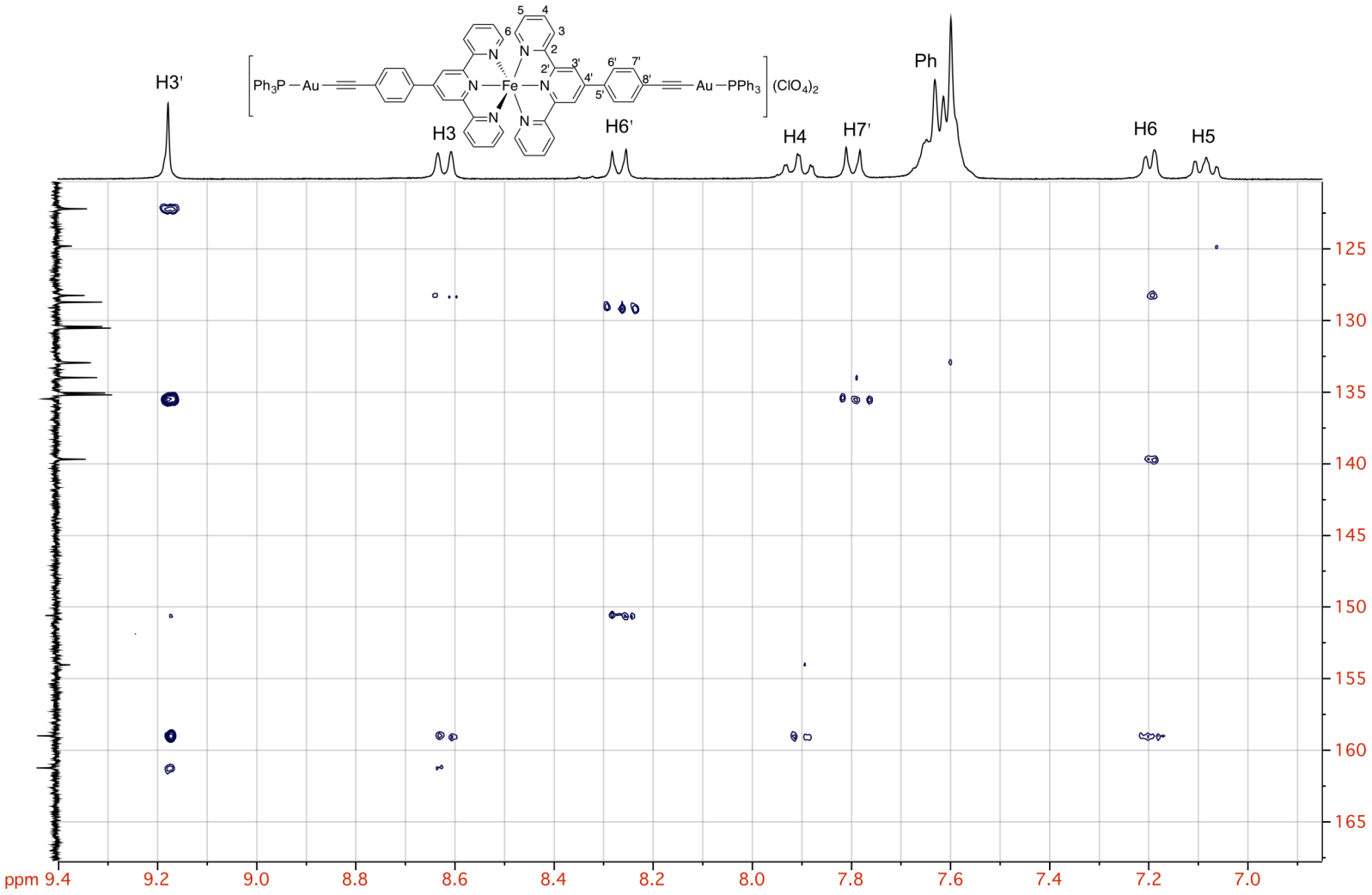

Figure S11. HMBC (300.1 MHz, CD_3CN) spectrum of $[Fe(TpylC_6H_4C{\equiv}CAuPPh_3)_2](ClO_4)_2$.

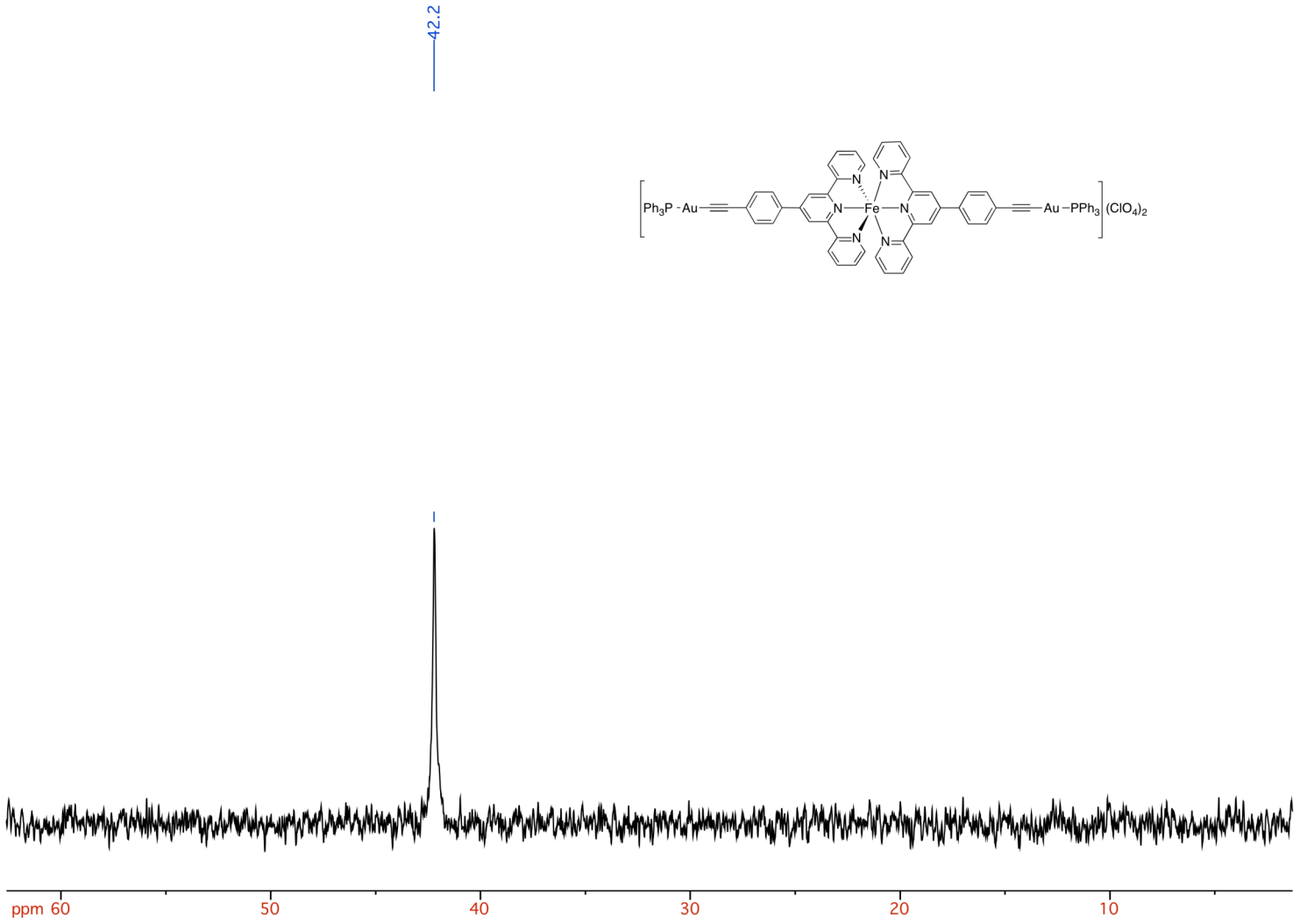

Figure S12. $^{31}P\{^{1}H\}$ NMR (121.5 MHZ, CD_3CN) spectrum of $[Fe(TpylC_6H_4C{\equiv}CAuPPh_3)_2](ClO_4)_2$.

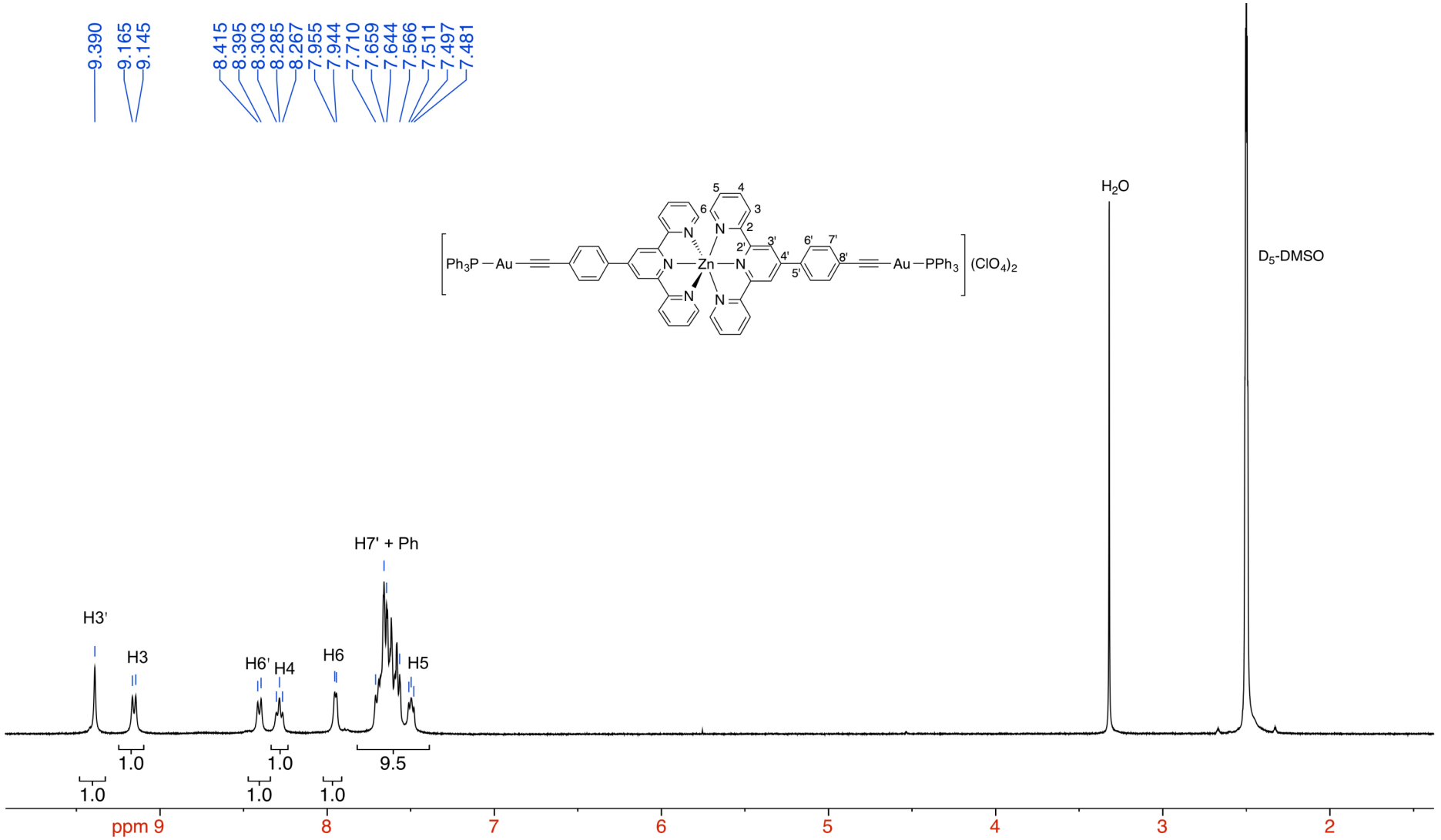

Figure S13. ^{1}H NMR (400.9 MHz, D_6-DMSO) spectrum of $[Zn(TpylC_6H_4C{\equiv}CAuPPh_3)_2](ClO_4)_2$.

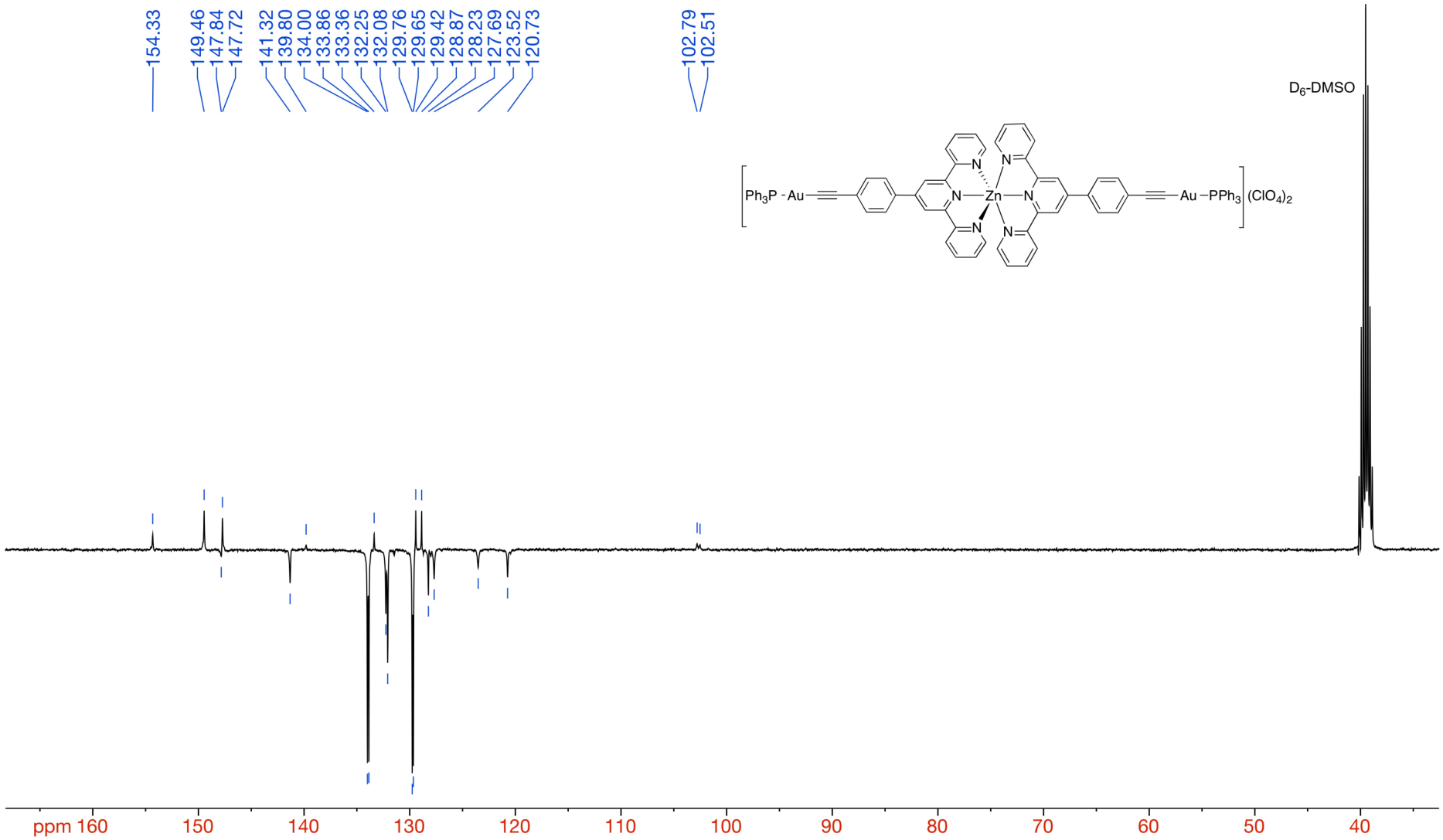

Figure S14. $^{13}C\{^{1}H\}$ NMR (100.8 MHz, D_6-DMSO) spectrum of $[Zn(TpylC_6H_4C{\equiv}CAuPPh_3)_2](ClO_4)_2$.

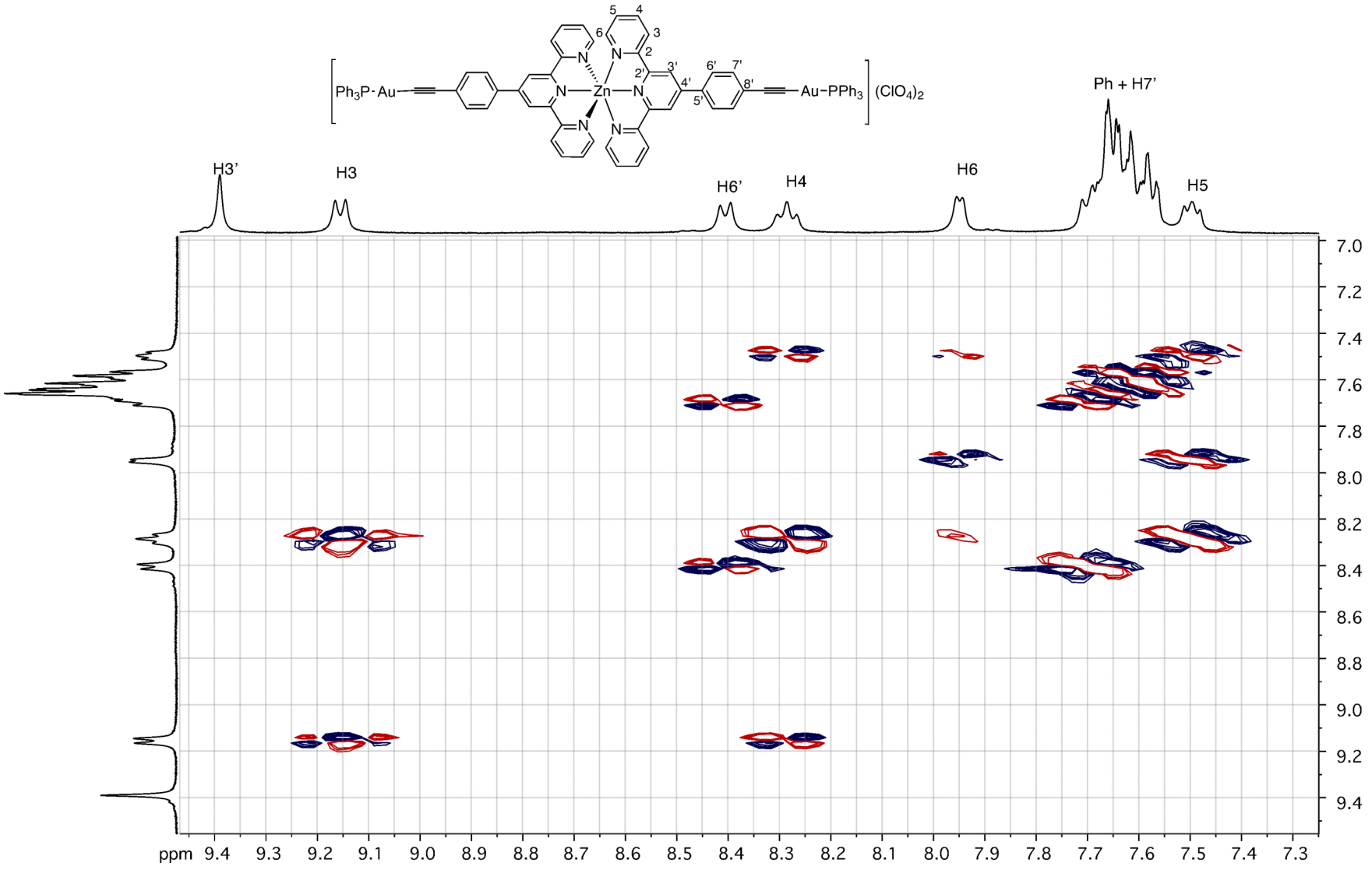

Figure S15. COSY (400.9 MHz, D_6-DMSO) spectrum of $[Zn(TpylC_6H_4C{\equiv}CAuPPh_3)_2](ClO_4)_2$.

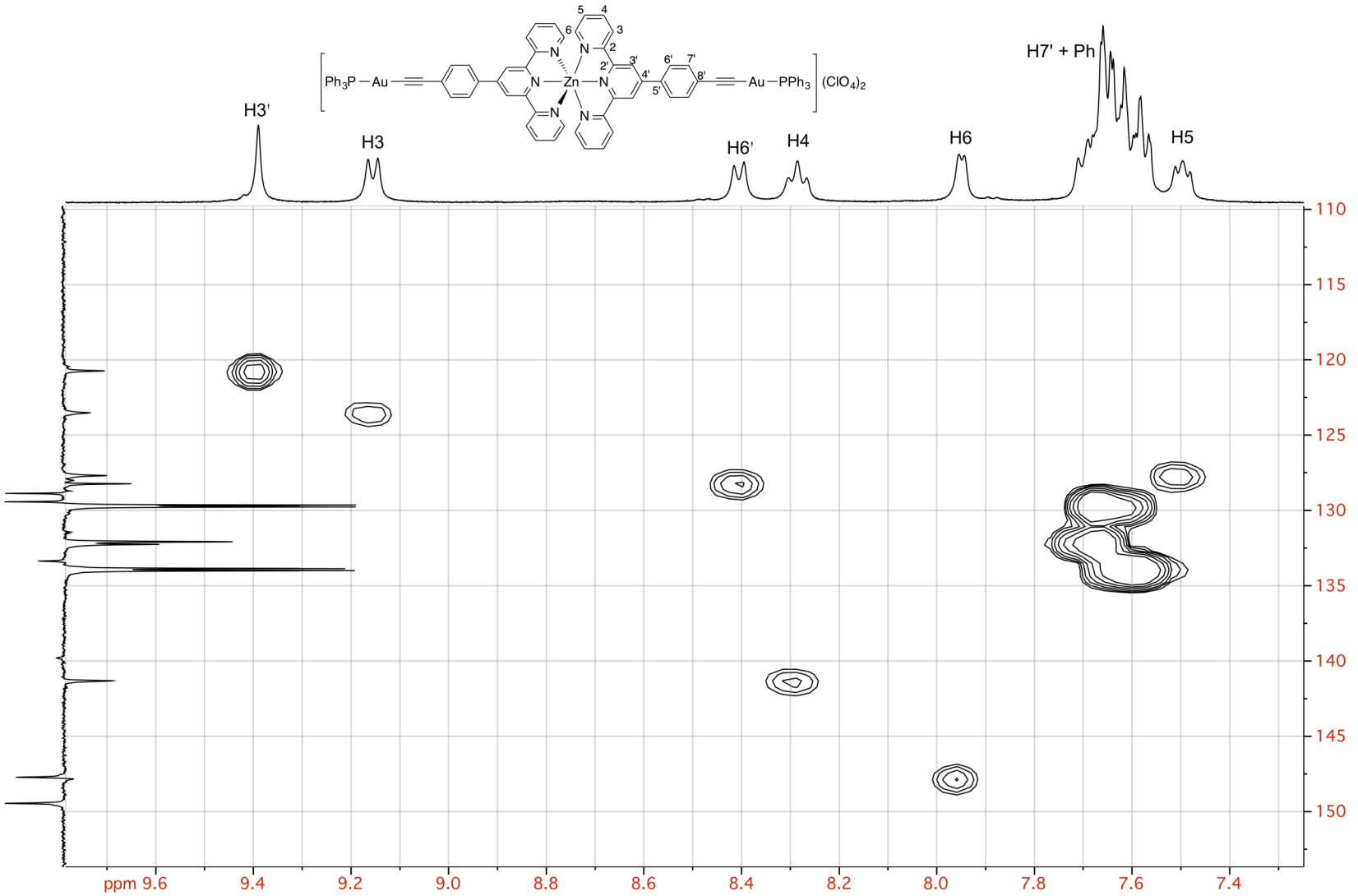

Figure S16. HMQC (400.9 MHz, D_6-DMSO) spectrum of $[Zn(TpylC_6H_4C{\equiv}CAuPPh_3)_2](ClO_4)_2$.

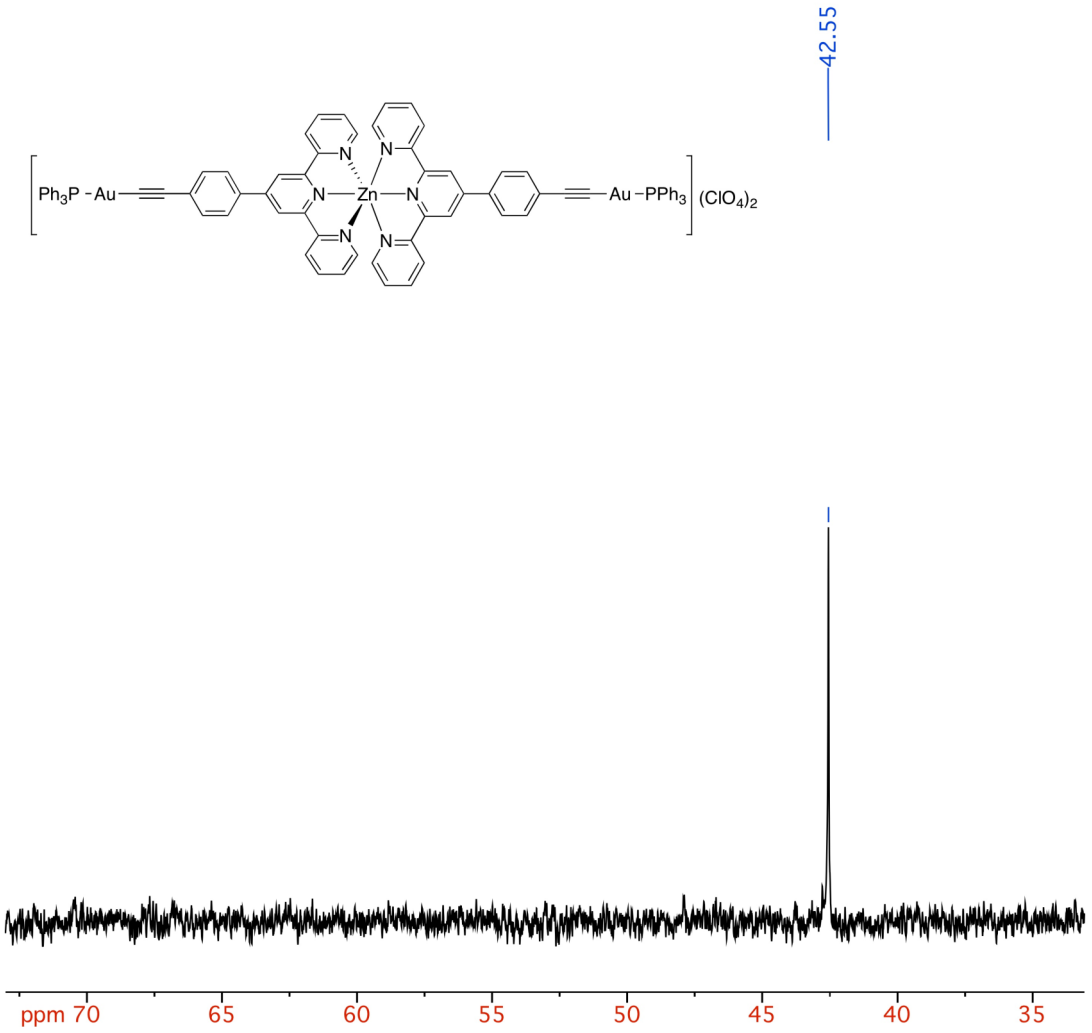

Figure S17. $^{31}P\{^{1}H\}$ NMR (162.3 MHz, D_6-DMSO) spectrum of $[Zn(TpylC_6H_4C{\equiv}CAuPPh_3)_2](ClO_4)_2$.

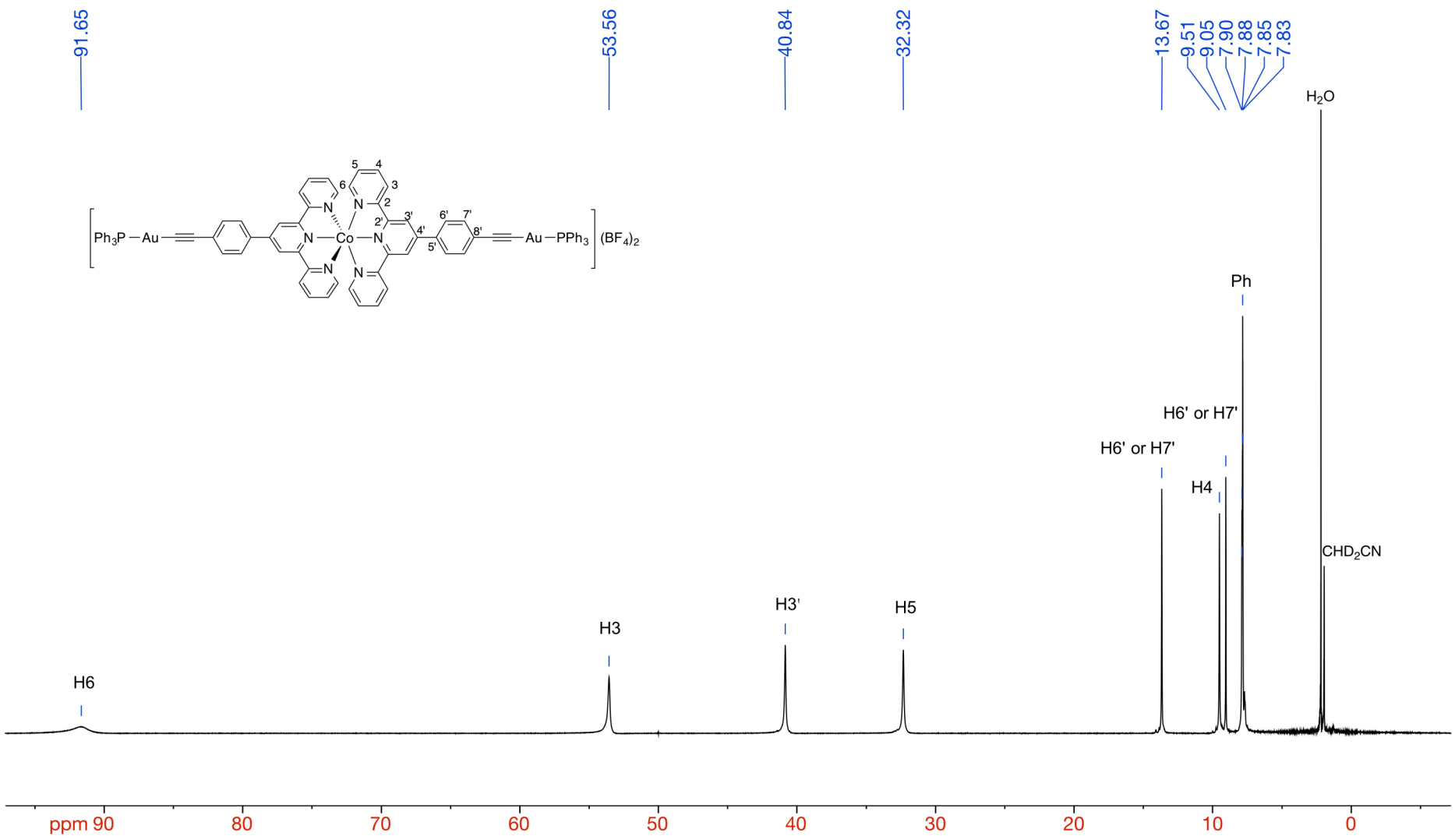

Figure S18. ^{1}H NMR (400.9 MHz, CD_3CN) spectrum of $[Co(TpylC_6H_4C{\equiv}CAuPPh_3)_2](BF_4)_2$.

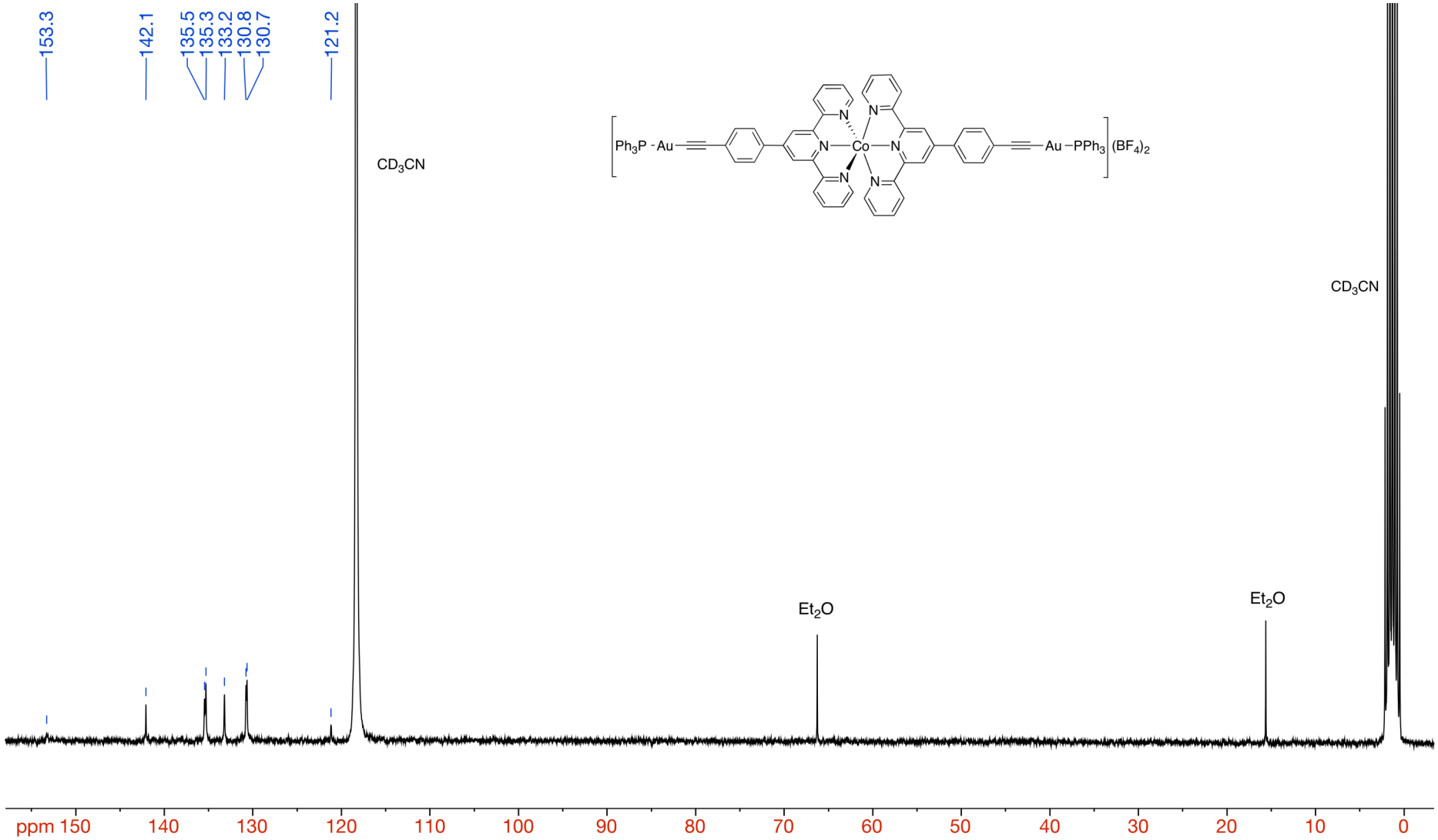

Figure S19. $^{13}C\{^{1}H\}$ NMR (75.5 MHZ, CD_3CN) spectrum of $[Co(TpylC_6H_4C{\equiv}CAuPPh_3)_2](BF_4)_2$.

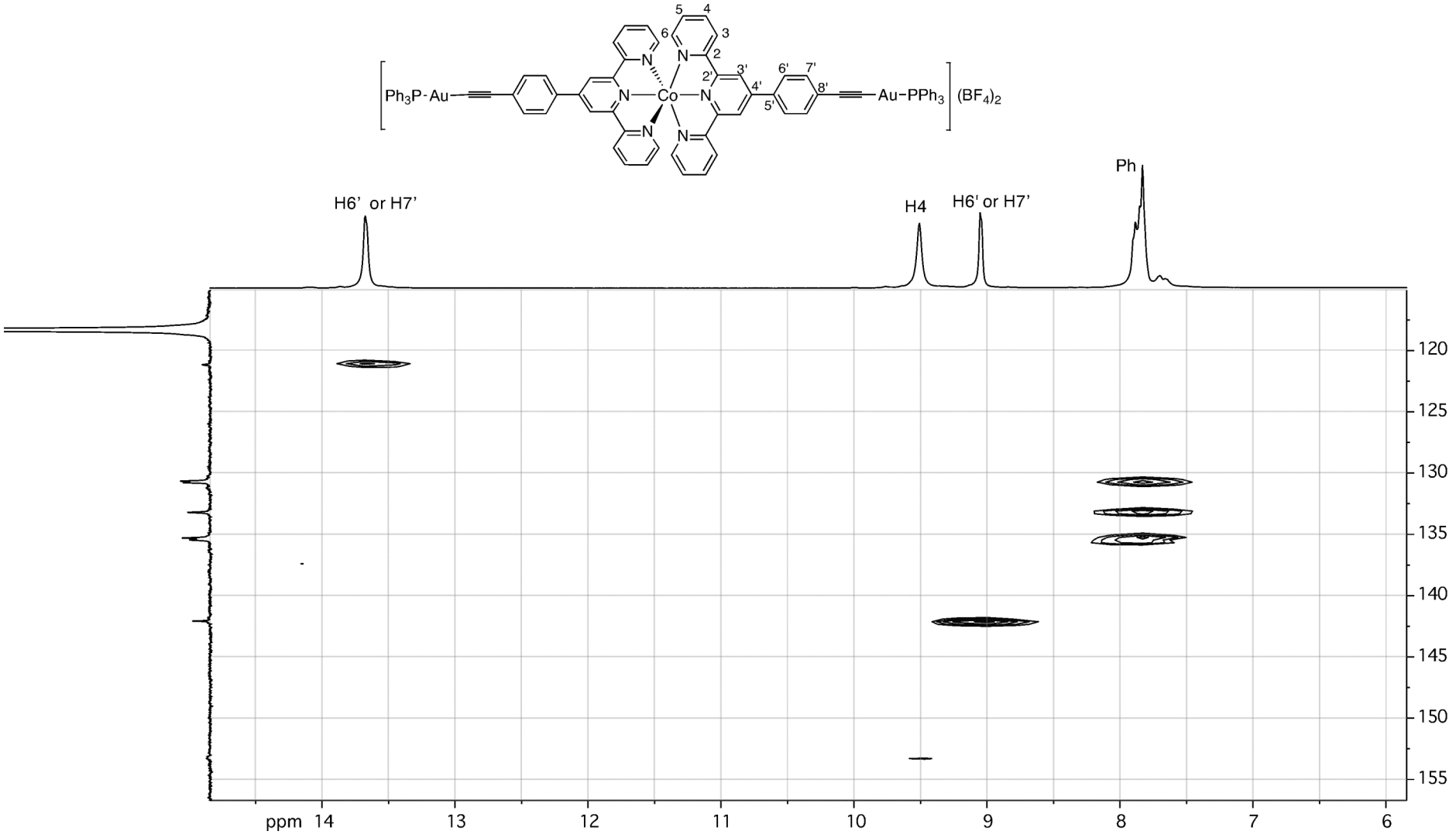

Figure S20. HMQC (300.1 MHZ, CD_3CN) spectrum of $[Co(TpylC_6H_4C{\equiv}CAuPPh_3)_2](BF_4)_2$.

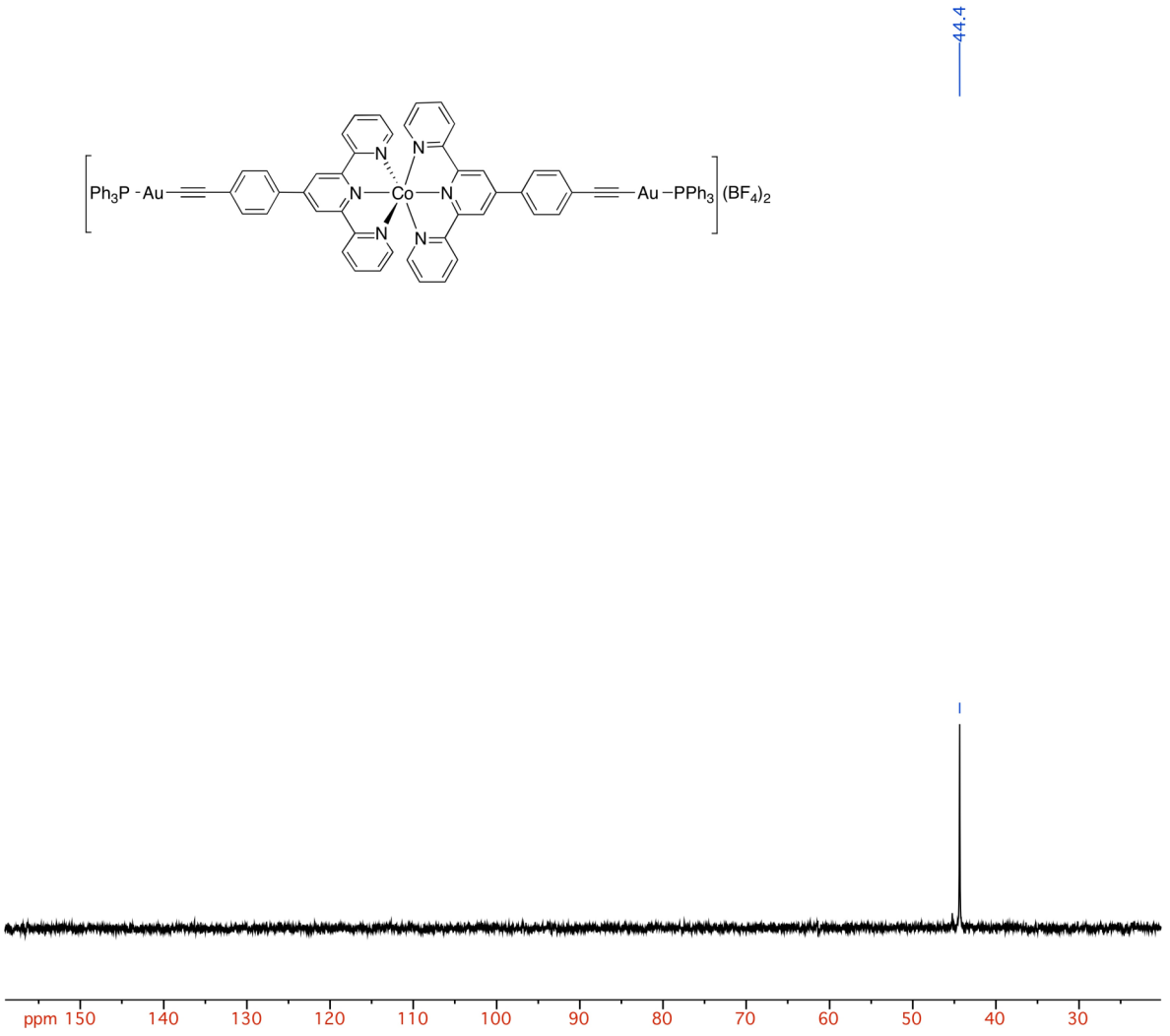

Figure S21. $^{31}P\{^{1}H\}$ NMR (162.29 MHz, CD_3CN) spectrum of $[Co(TpylC_6H_4C{\equiv}CAuPPh_3)_2](BF_4)_2$ in CD_3CN.

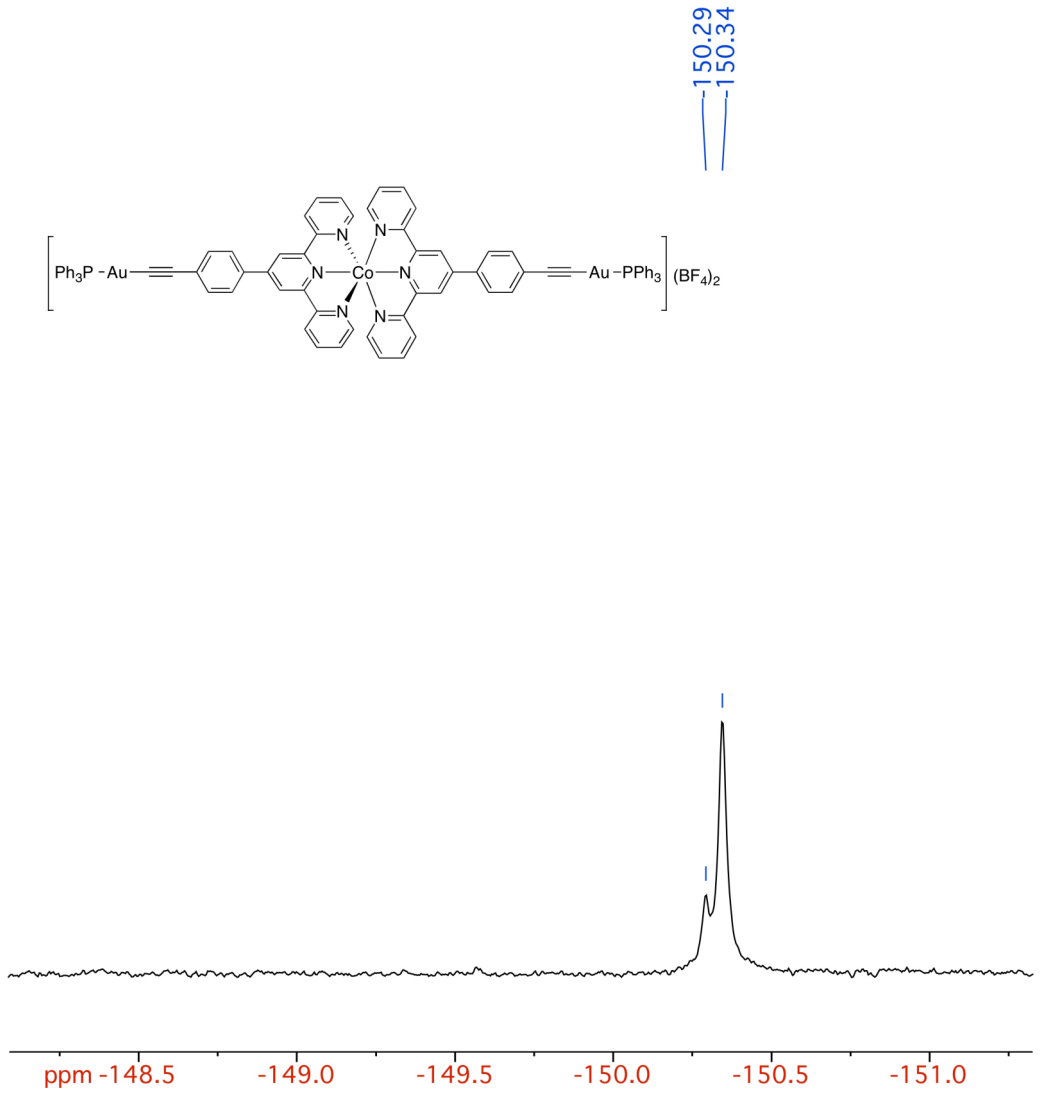

Figure S22. ^{19}F NMR (282.4 MHz, CD_3CN) spectrum of $[Co(TpylC_6H_4C{\equiv}CAuPPh_3)_2](BF_4)_2$.

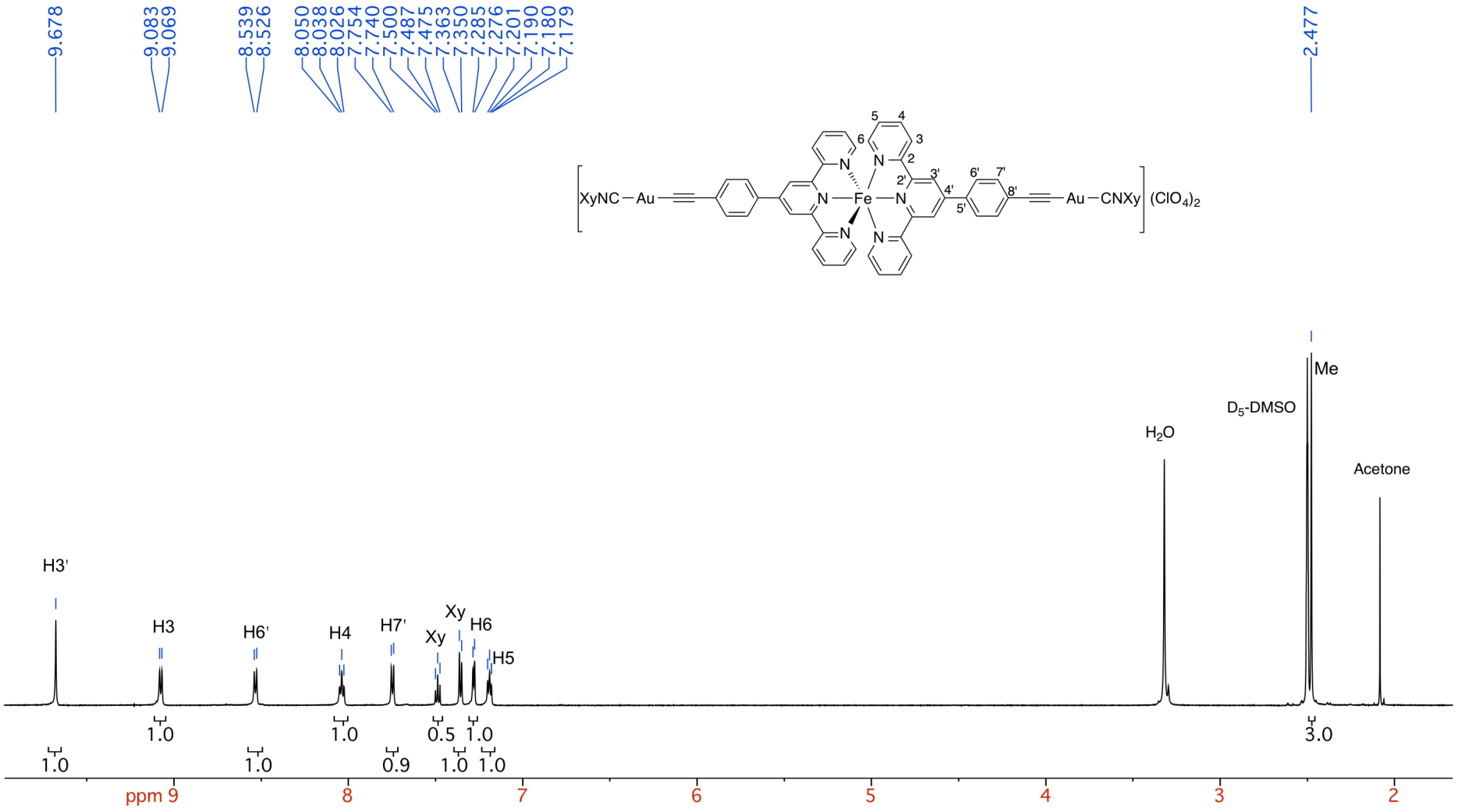

Figure S23. ^{1}H NMR (600.2 MHz, D_6-DMSO) spectrum of $[Fe(TpylC_6H_4C{\equiv}CAuCNXy)_2](ClO_4)_2$.

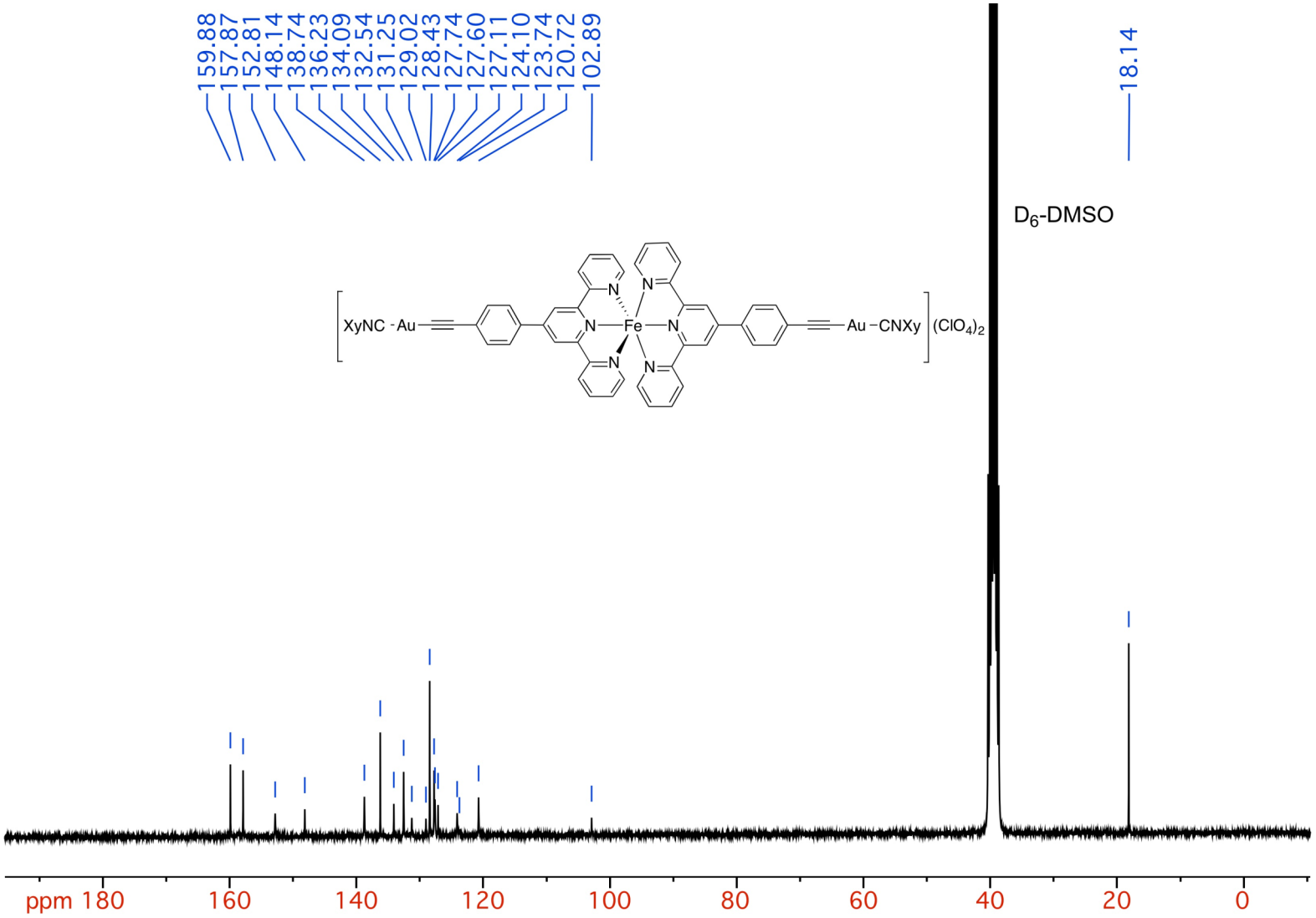

Figure S24. $^{13}C\{^{1}H\}$ NMR (75.5 MHz, D_6-DMSO) spectrum of $[Fe(TpylC_6H_4C{\equiv}CAuCNXy)_2](ClO_4)_2$.

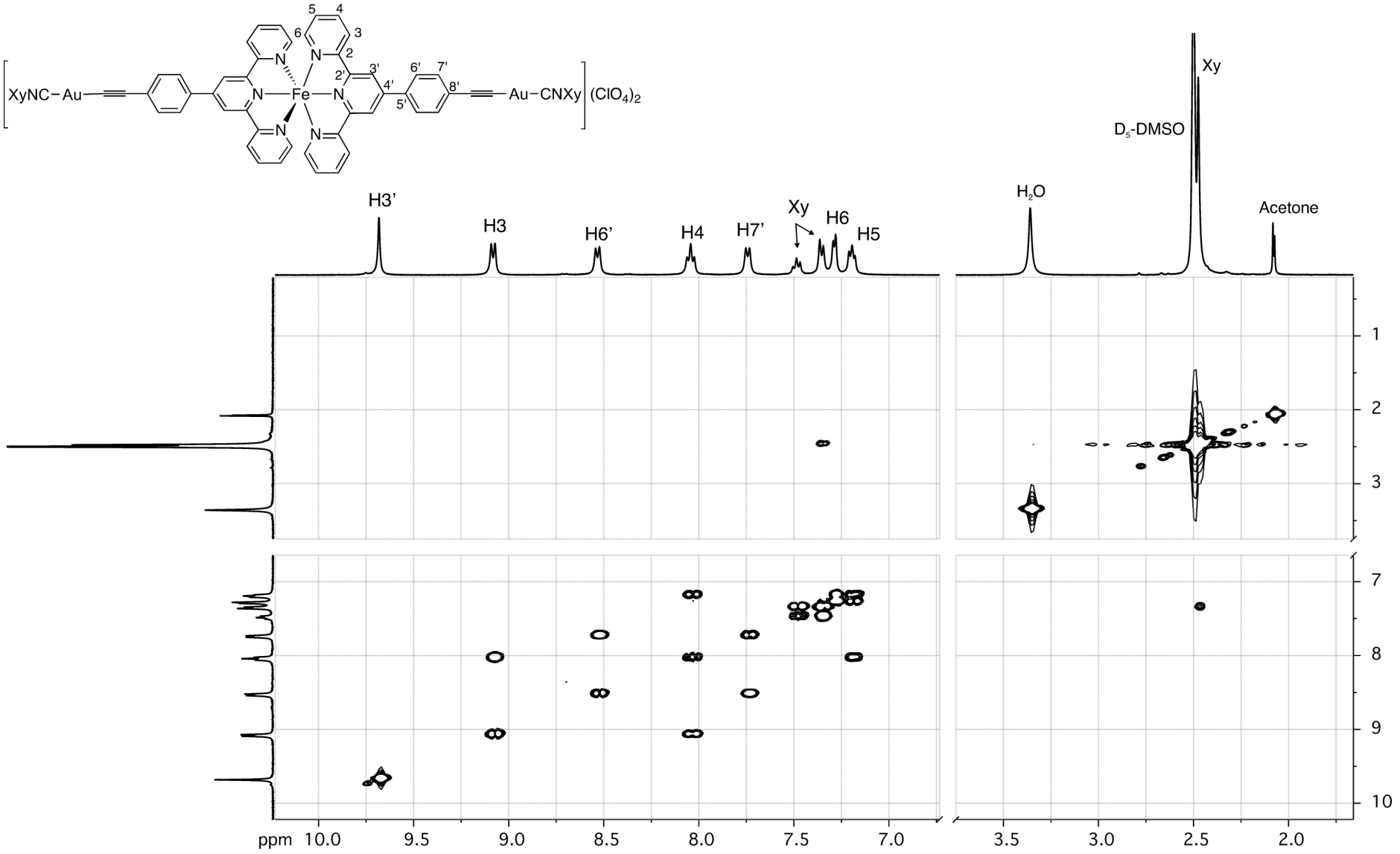

Figure S25. COSY (400.9 MHz, D_6-DMSO) spectrum of $[Fe(TpylC_6H_4C{\equiv}CAuCNXy)_2](ClO_4)_2$.

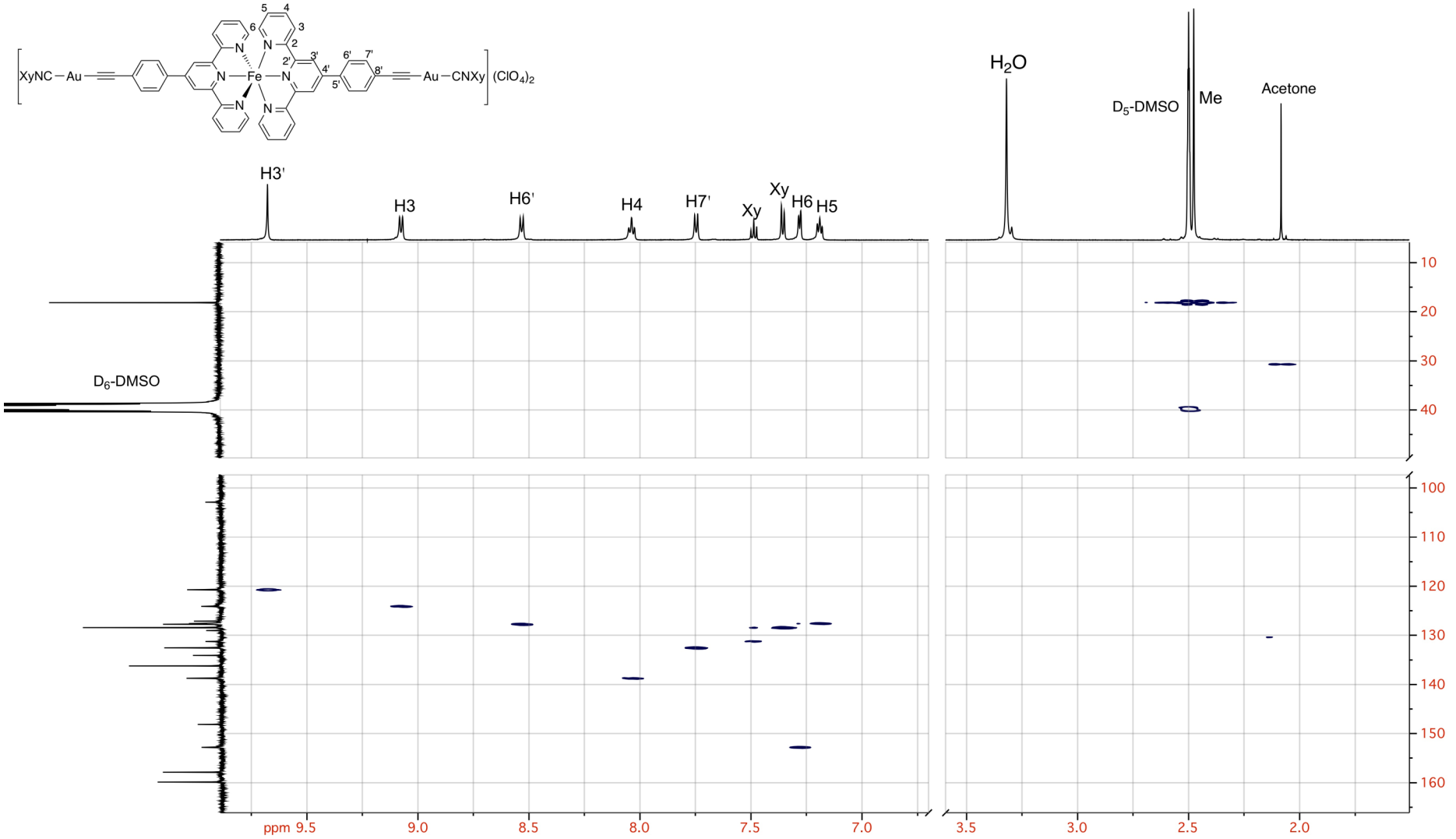

Figure S26. HMQC (600.1 MHz, D_6-DMSO) spectrum of $[Fe(TpylC_6H_4C{\equiv}CAuCNXy)_2](ClO_4)_2$.

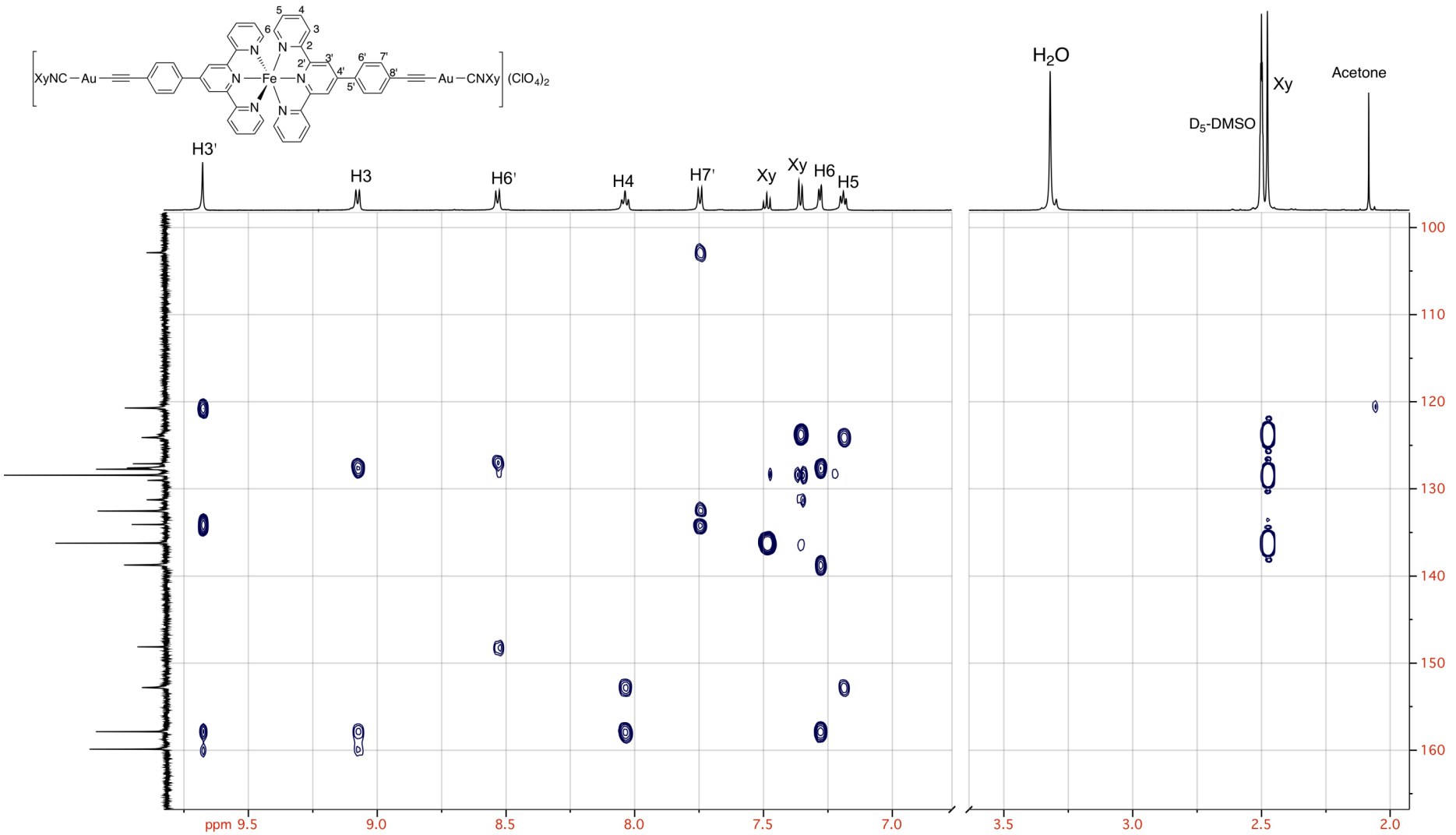

Figure S27. HMBC (600.1 MHz, D_6-DMSO) spectrum of $[Fe(TpylC_6H_4C{\equiv}CAuCNXy)_2](ClO_4)_2$.

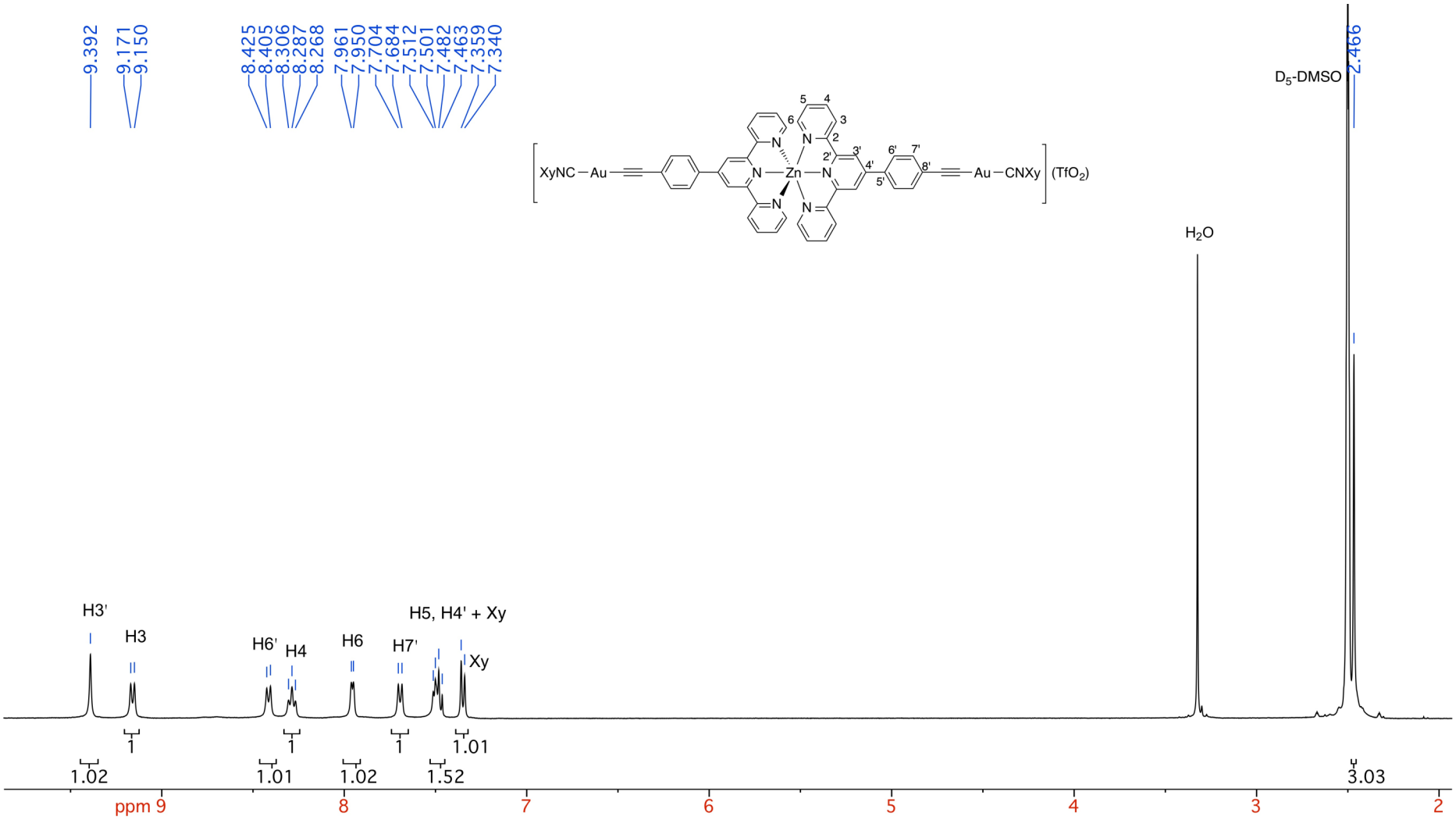

Figure S28. ^{1}H NMR (400.9 MHz, D_6-DMSO) spectrum of $[Zn(TpylC_6H_4C{\equiv}CAuCNXy)_2](TfO)_2$.

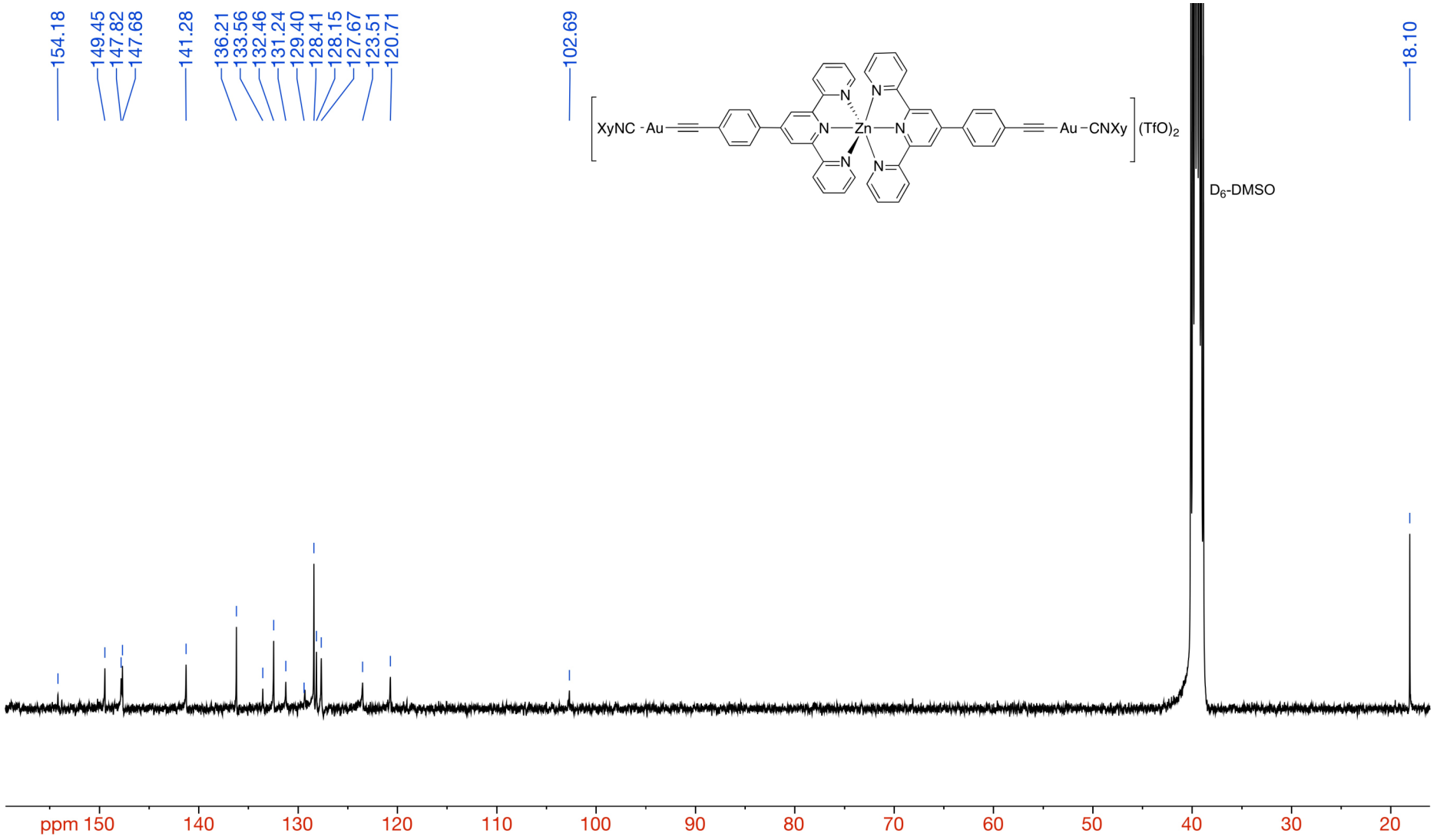

Figure S29. $^{13}C\{^{1}H\}$ NMR (100.8 MHz, D_6-DMSO) spectrum of $[Zn(TpylC_6H_4C{\equiv}CAuCNXy)_2](TfO)_2$.

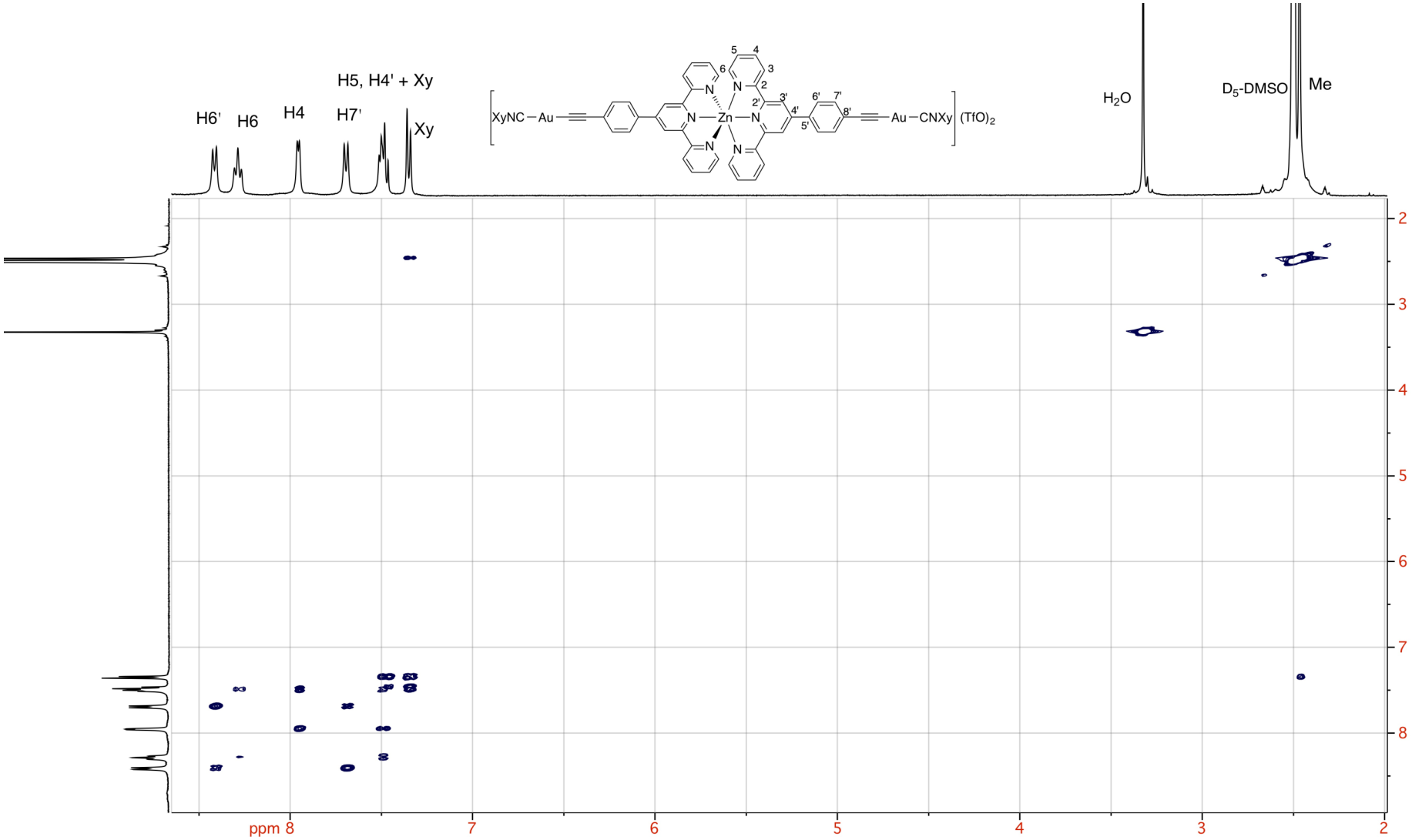

Figure S30. COSY (400.9 MHz, D_6-DMSO) spectrum of $[Zn(TpylC_6H_4C{\equiv}CAuCNXy)_2](TfO)_2$.

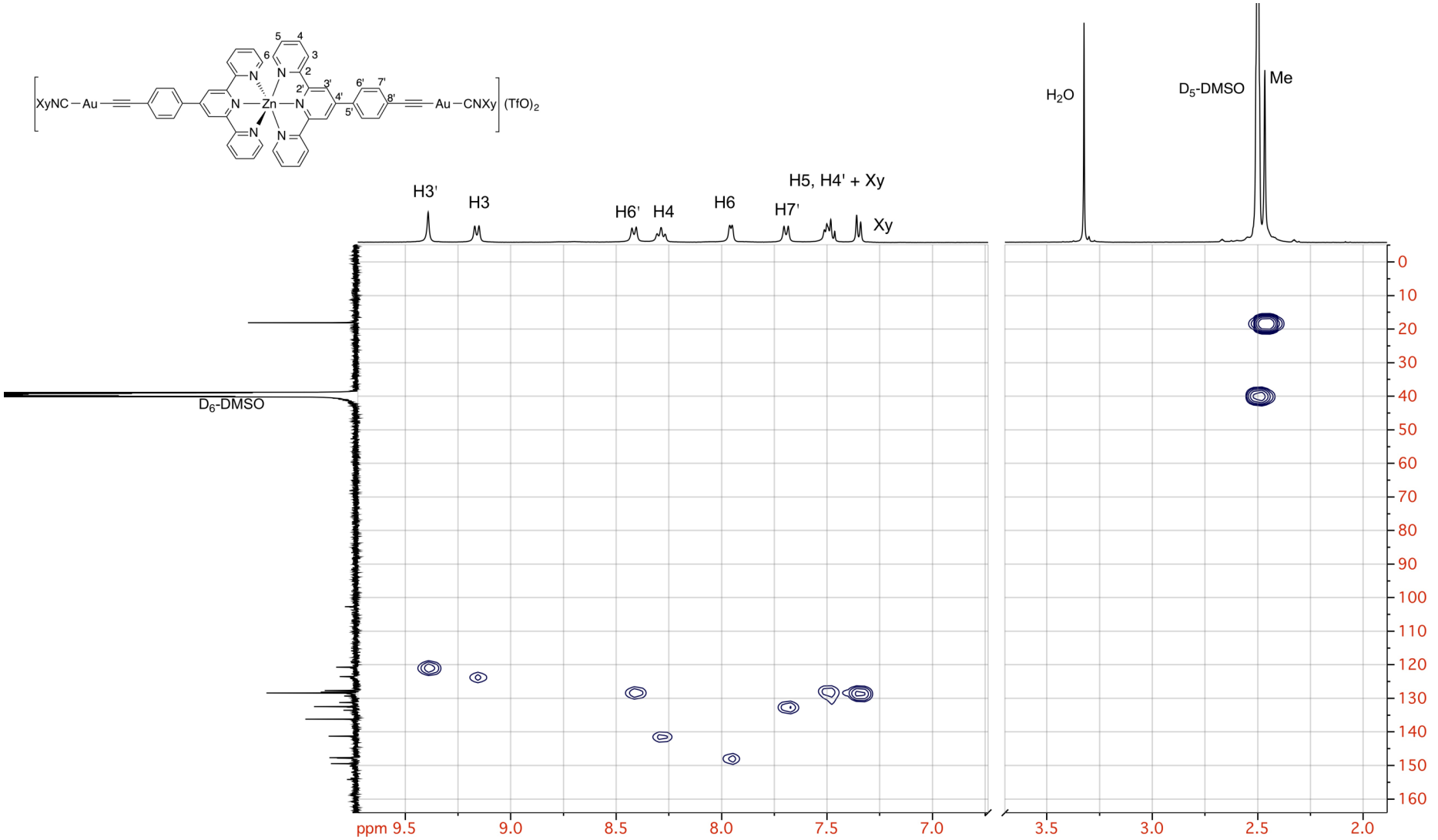

Figure S31. HMQC (400.9 MHz, D_6-DMSO) spectrum of $[Zn(TpylC_6H_4C{\equiv}CAuCNXy)_2](TfO)_2$.

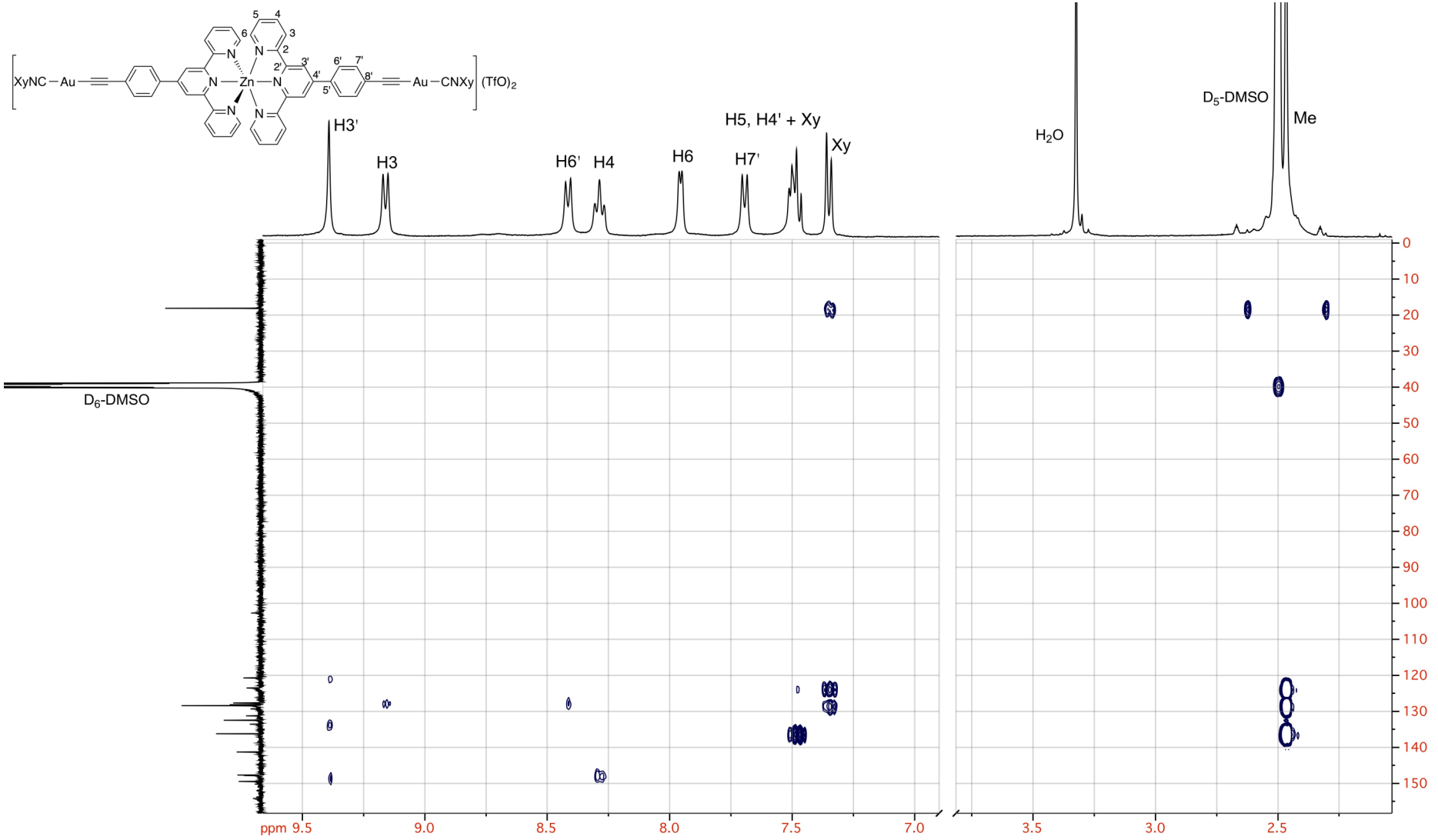

Figure S32. HMBC (400.9 MHz, D_6-DMSO) spectrum of $[Zn(TpylC_6H_4C{\equiv}CAuCNXy)_2](TfO)_2$.

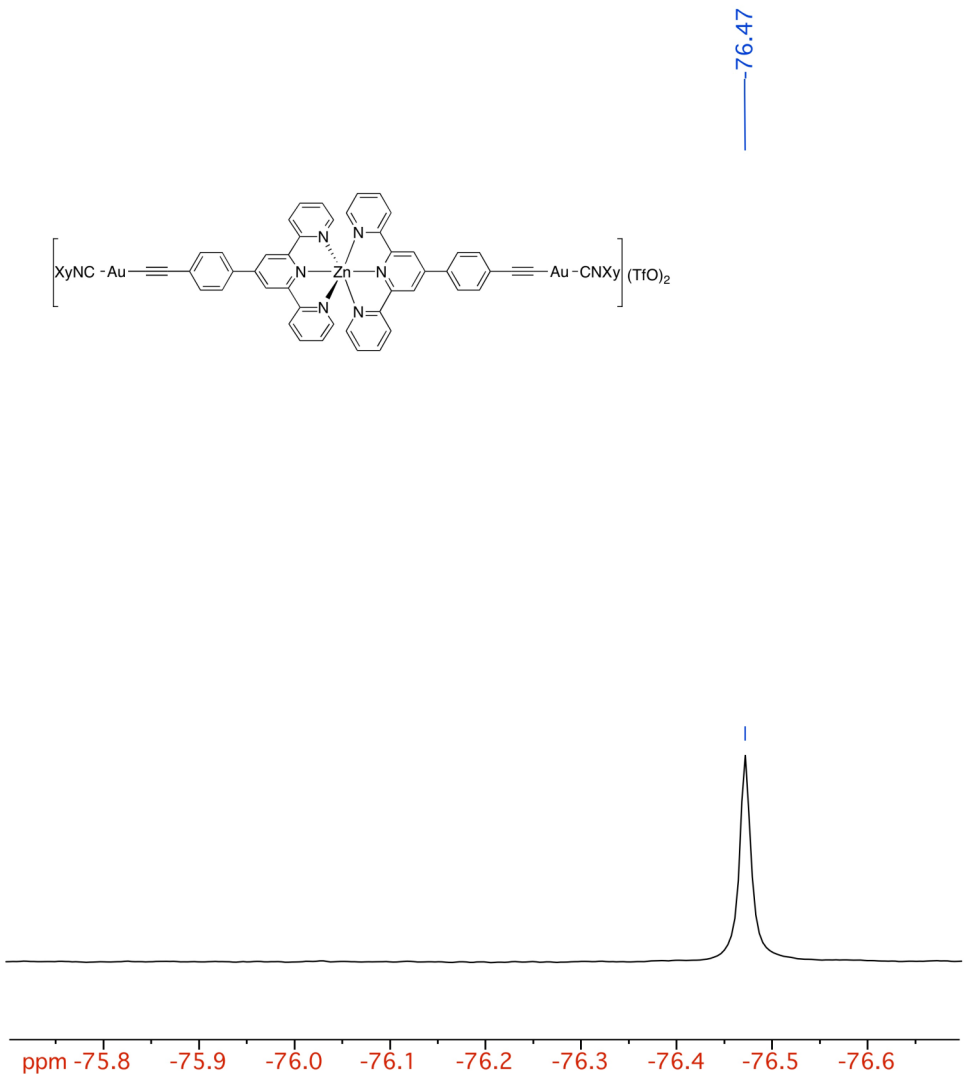

Figure S33. ^{19}F NMR (282.4 MHz, D_6-DMSO) spectrum of $[Zn(TpylC_6H_4C{\equiv}CAuCNXy)_2](TfO)_2$.

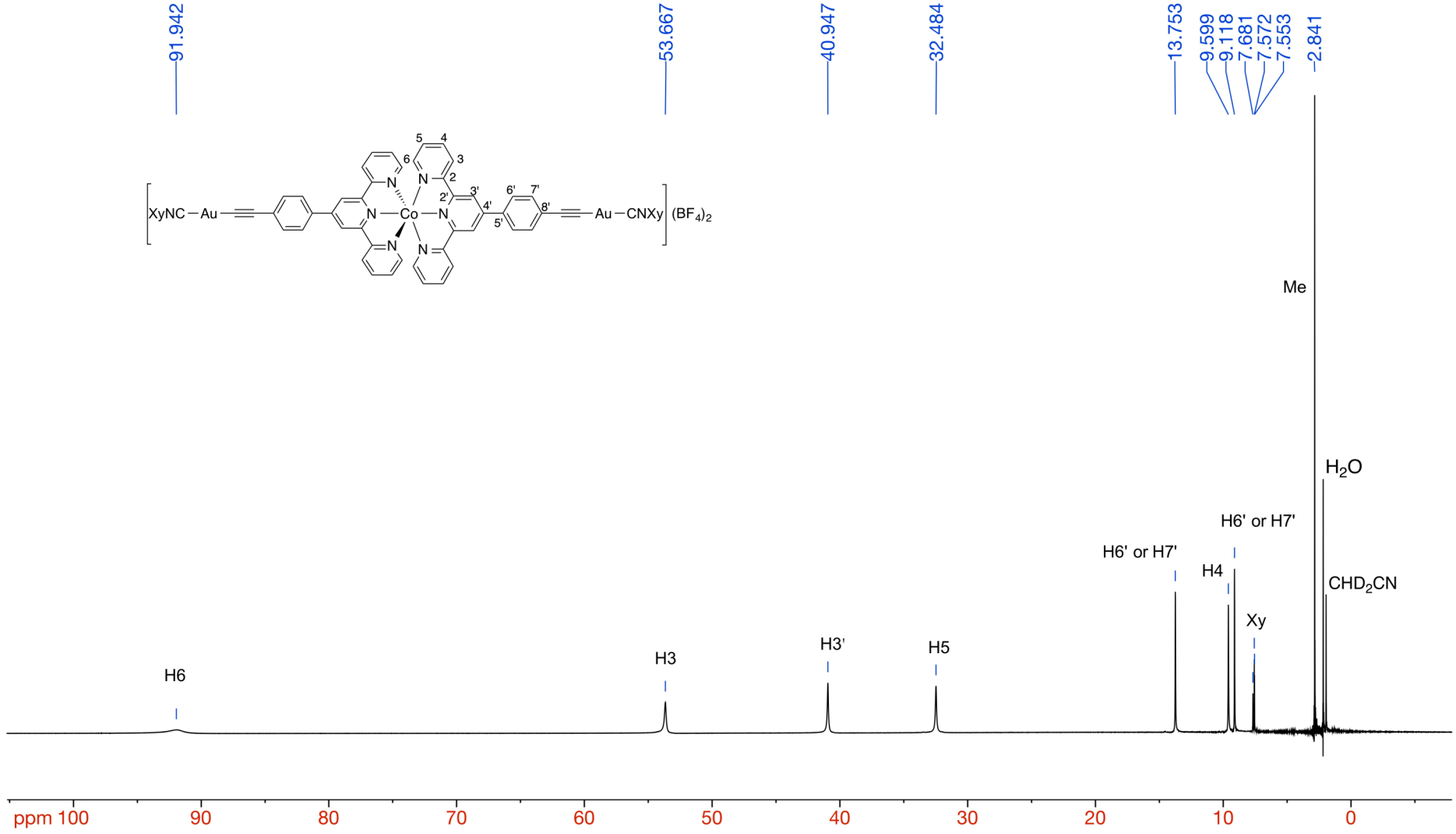

Figure S34. ^{1}H NMR (400.9 MHz, CD_3CN) spectrum of $[Co(TpylC_6H_4C{\equiv}CAuCNXy)_2](BF_4)_2$.

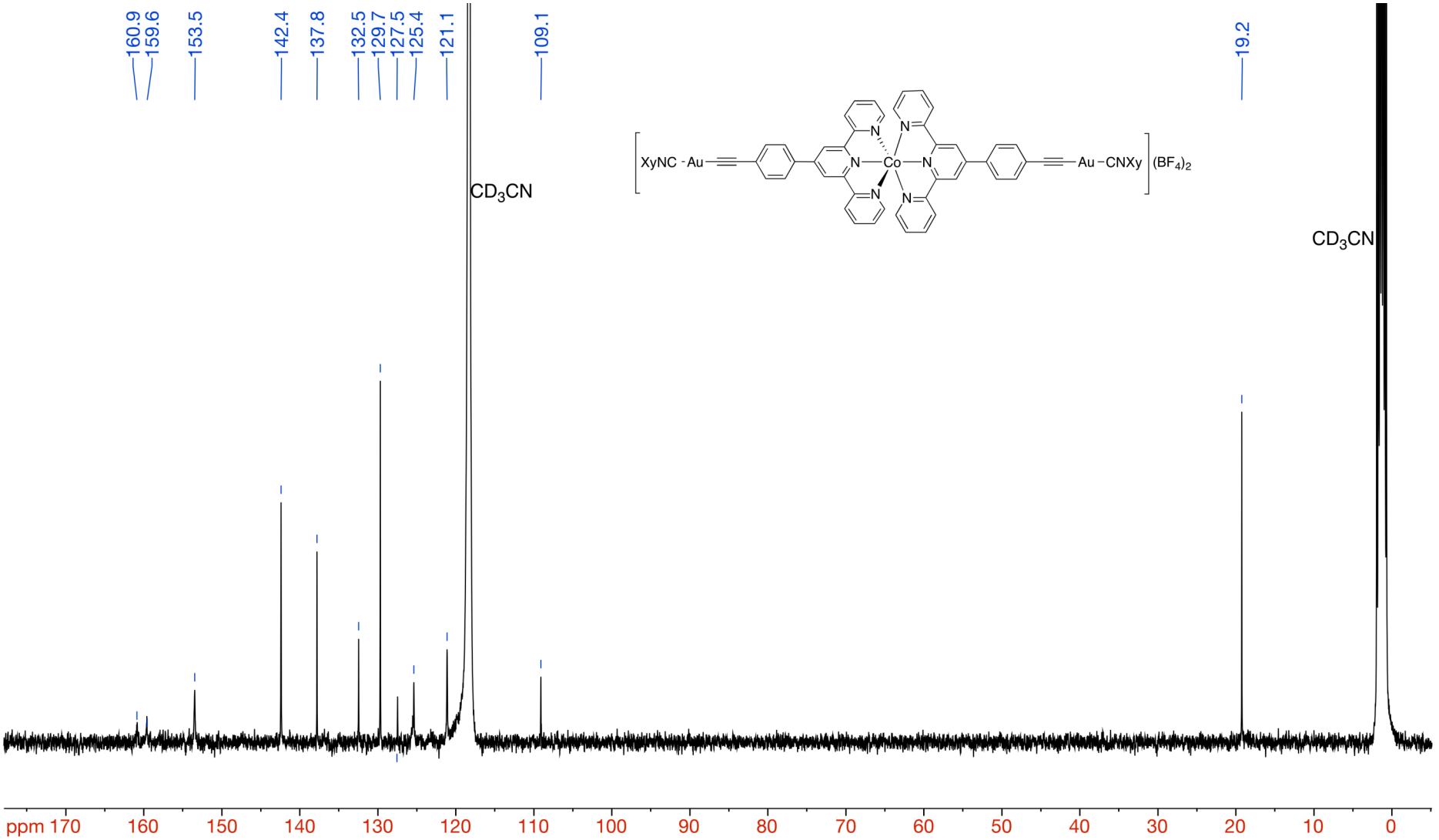

Figure S35. $^{13}C\{^{1}H\}$ NMR (100.8 MHz, CD_3CN) spectrum of $[Co(TpylC_6H_4C{\equiv}CAuCNXy)_2](BF_4)_2$.

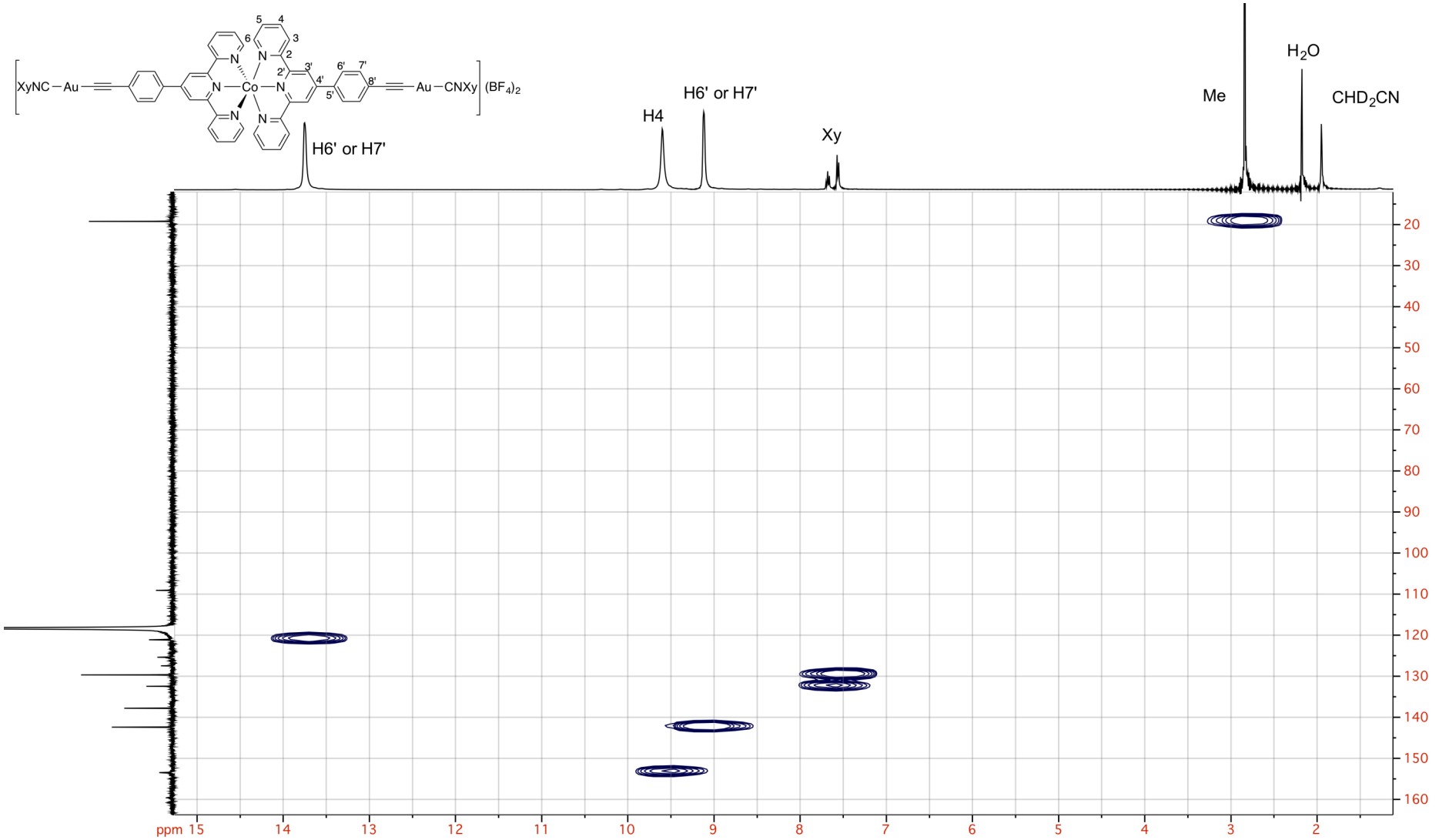

Figure S36. HMQC (400.9 MHz, D_6-DMSO) spectrum of $[Co(TpylC_6H_4C{\equiv}CAuCNXy)_2](BF_4)_2$.

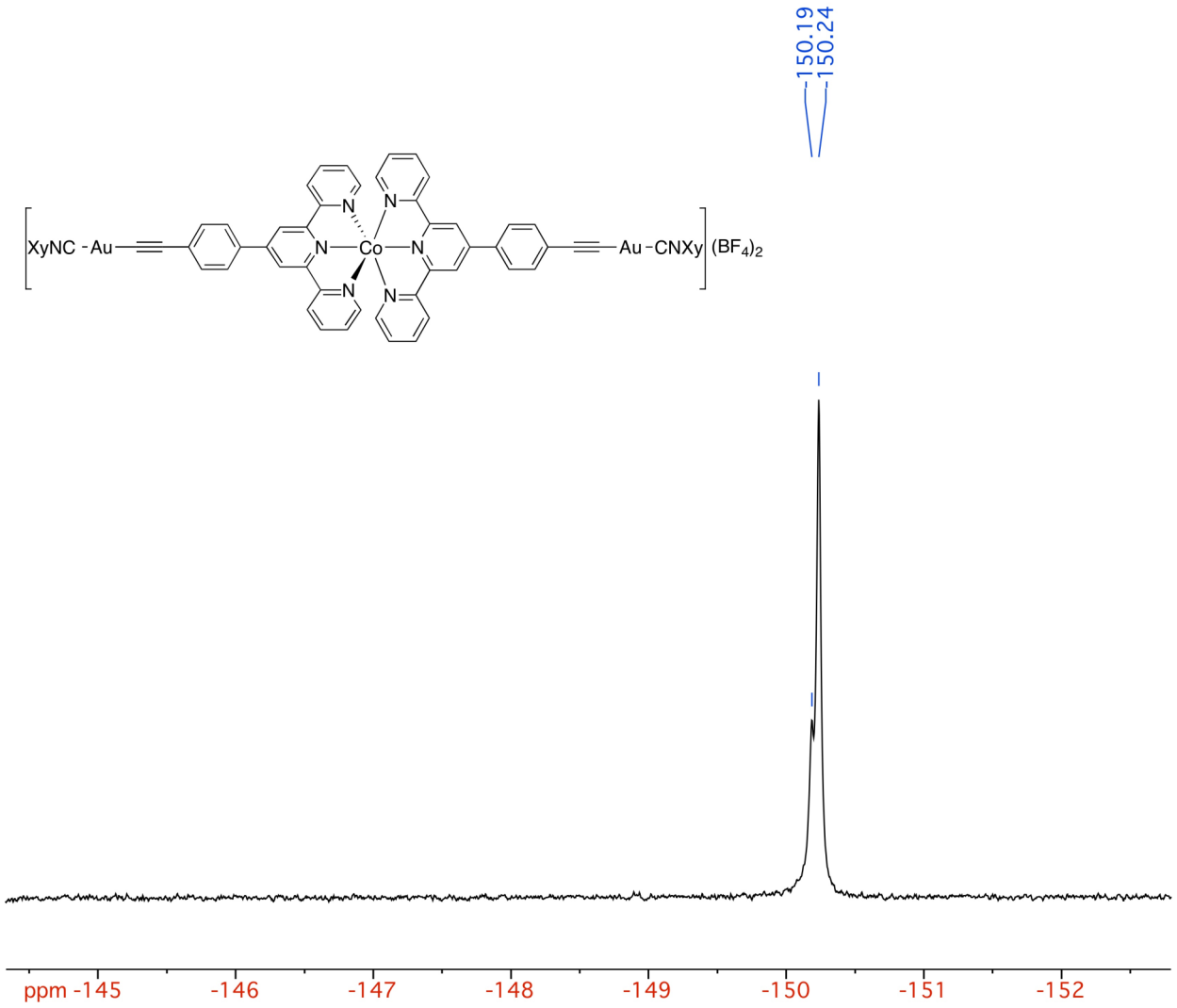

Figure S37. ^{19}F NMR (282.4 MHz, CD_3CN) spectrum of $[Co(TpylC_6H_4C{\equiv}CAuCNXy)_2](BF_4)_2$.

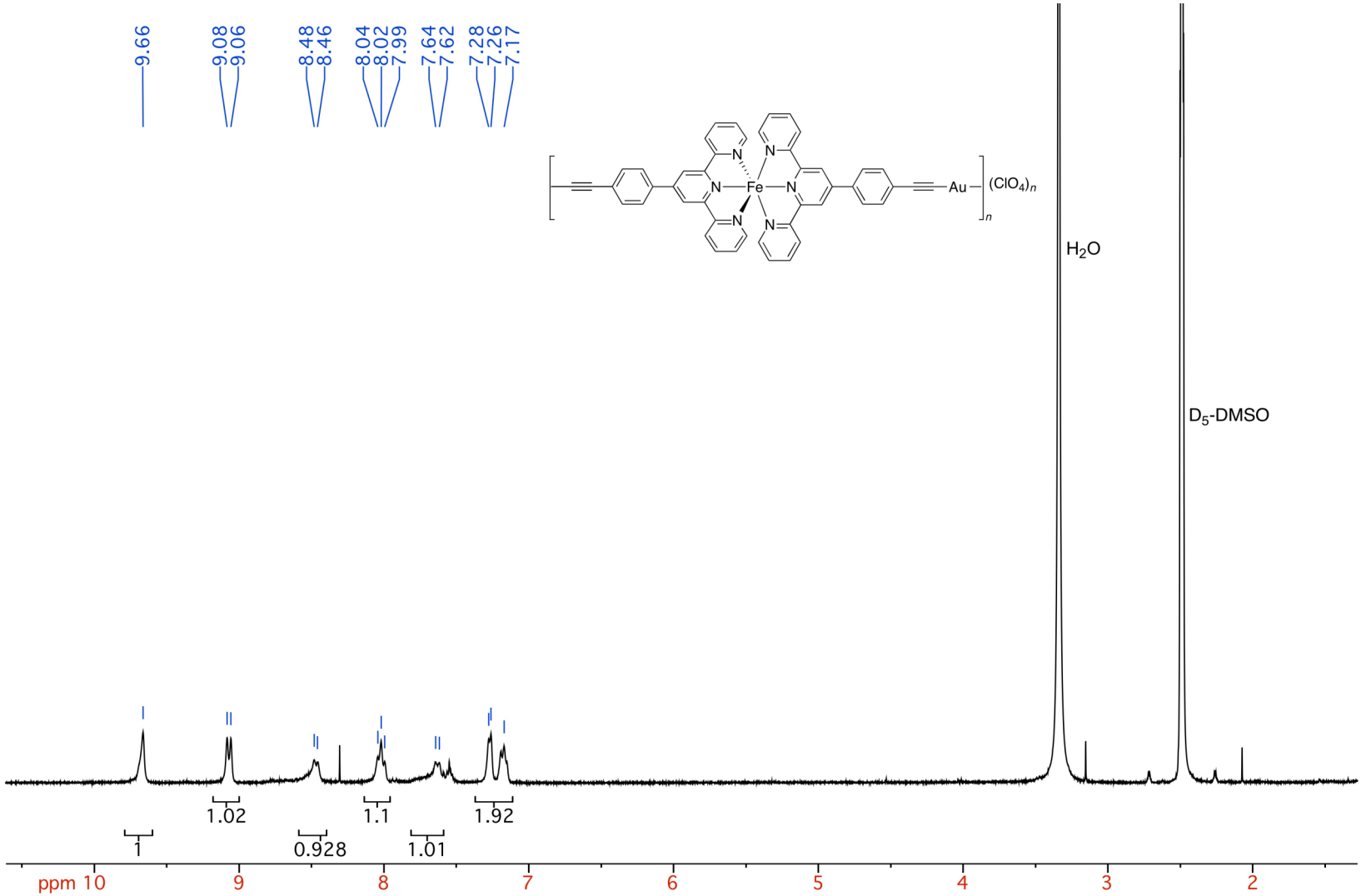

Figure S38. ^{1}H NMR (300.1 MHz, D_6-DMSO) spectrum of $[Fe\{(TpylC_6H_4C{\equiv}C)_2Au\}]_n(ClO_4)_n$. The small multiplet at ca. 7.5 ppm corresponds to a residual amount of $PPN(ClO_4)$.

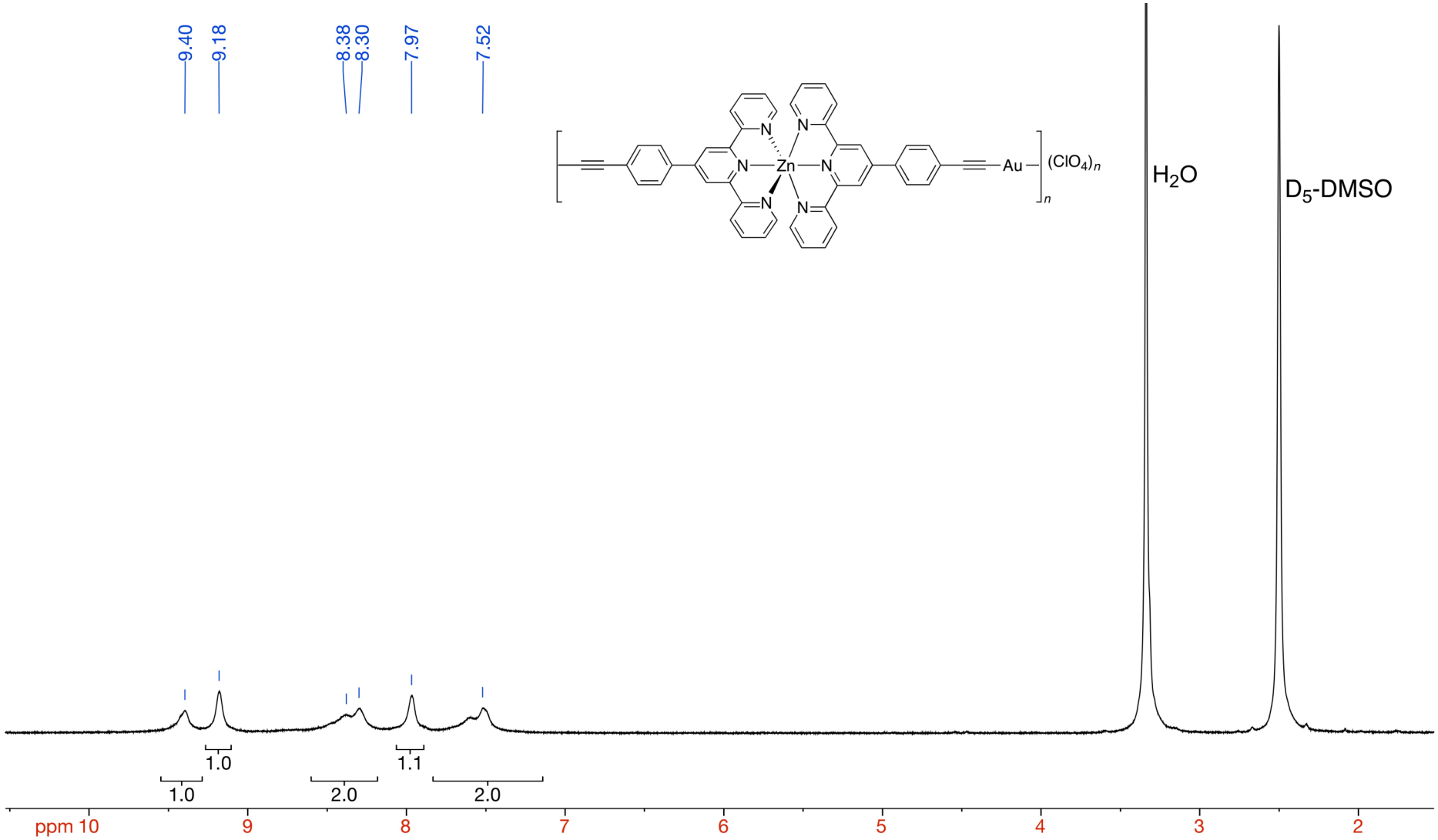

Figure S39. ^{1}H NMR (400.9 MHz, D_6-DMSO) spectrum of $[Zn\{(TpylC_6H_4C{\equiv}C)_2Au\}]_n(ClO_4)_n$.

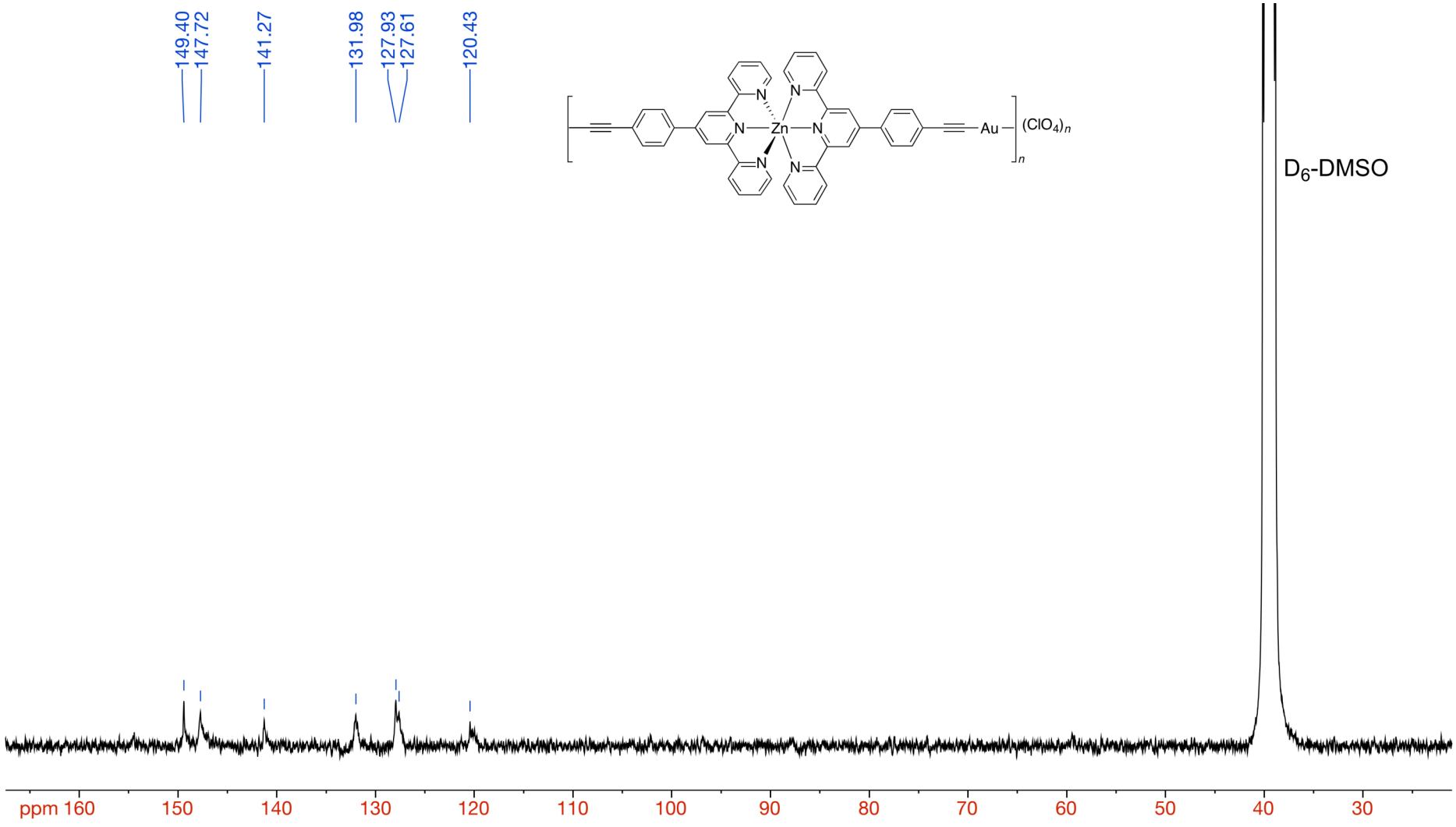

Figure S40. $^{13}C\{^{1}H\}$ NMR (100.8 MHz, D_6-DMSO) spectrum of $[Zn\{(TpylC_6H_4C{\equiv}C)_2Au\}]_n(ClO_4)_n$.

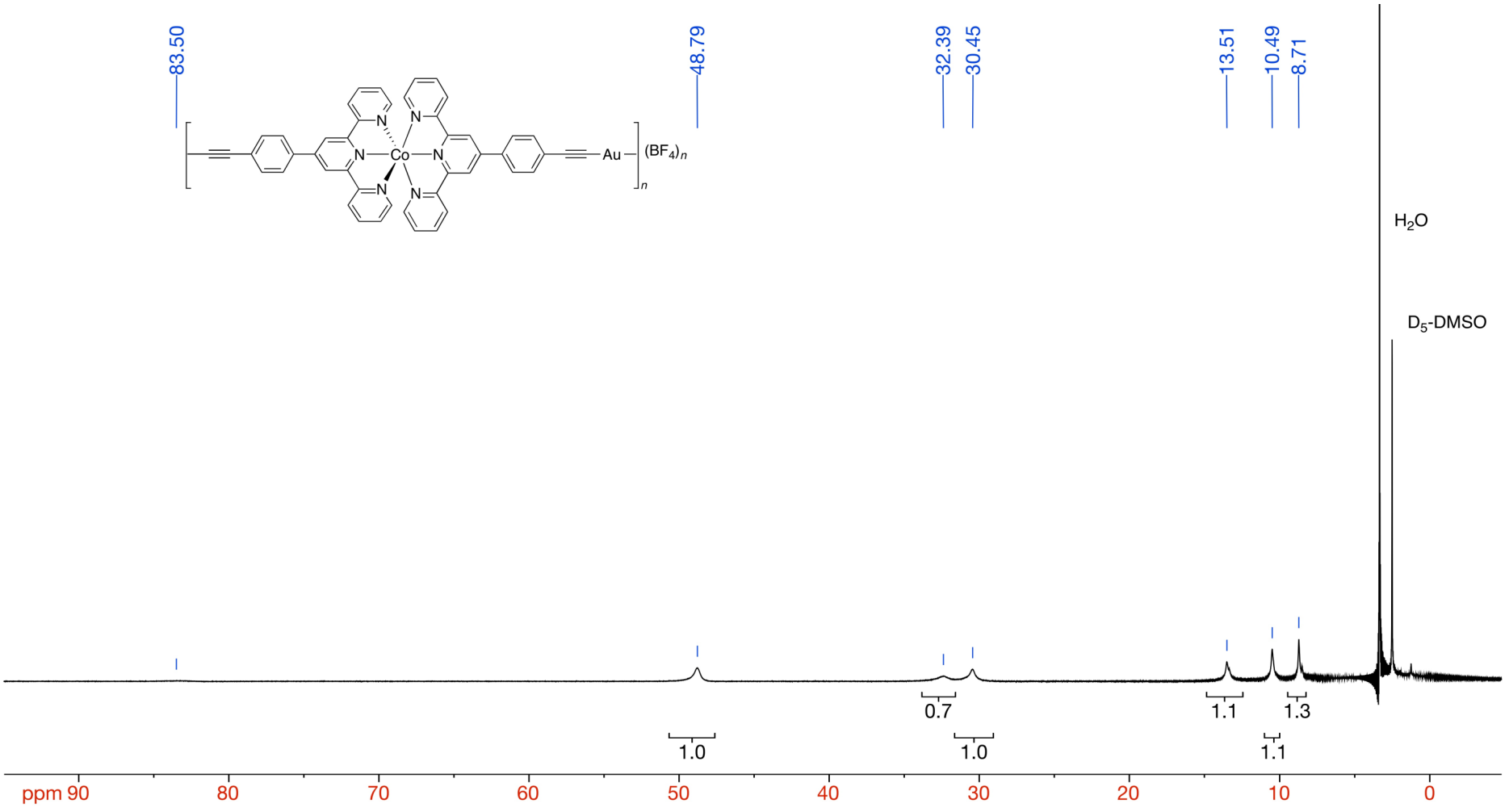

Figure S41. ^{1}H NMR (400.9 MHZ, D_6-DMSO) spectrum of $[Co\{(TpylC_6H_4C{\equiv}C)_2Au\}]_n(BF_4)_n$.

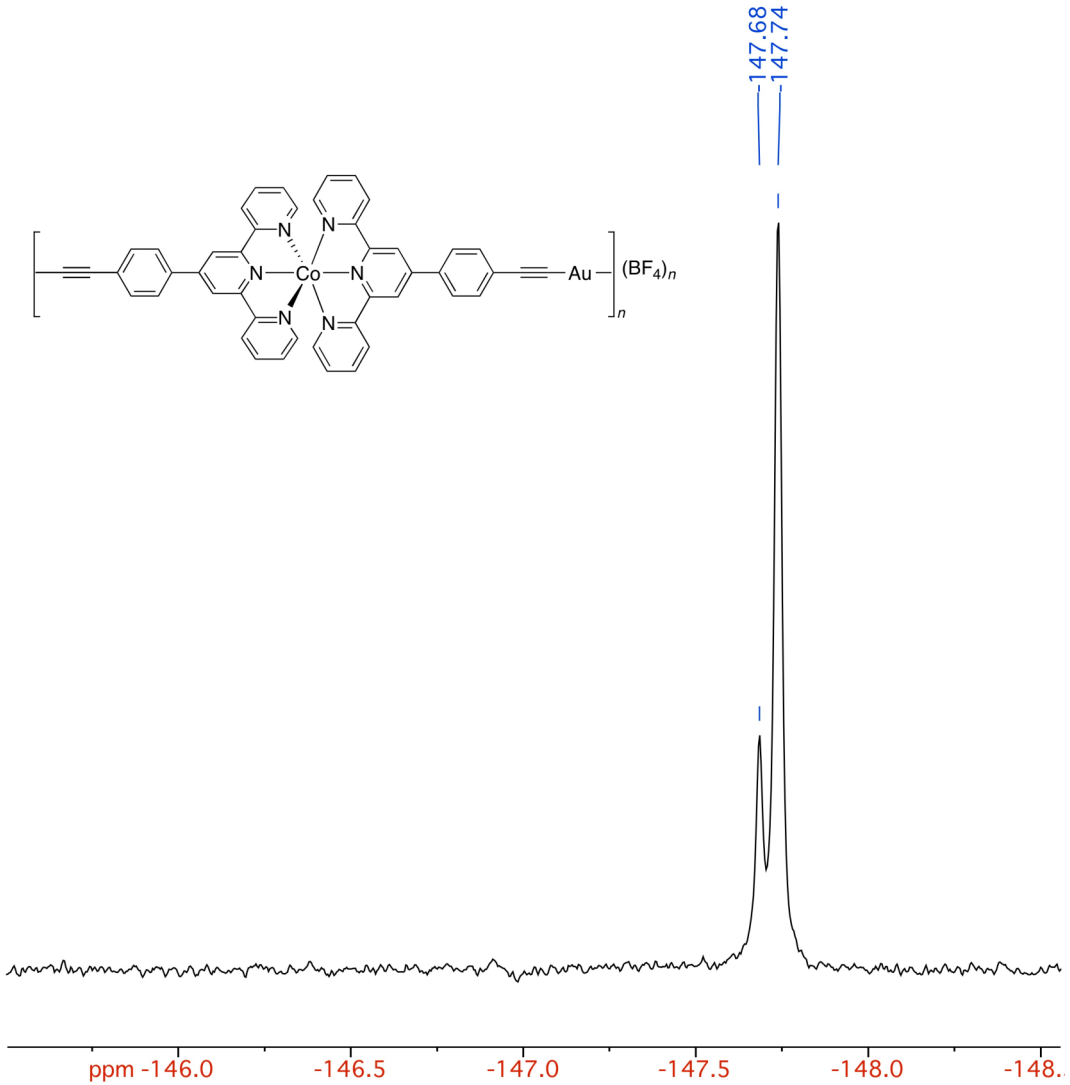

Figure S42. ^{19}F NMR (282.4 MHz, D_6-DMSO) spectrum of $[Co\{(TpylC_6H_4C{\equiv}C)_2Au\}]_n(BF_4)_n$.

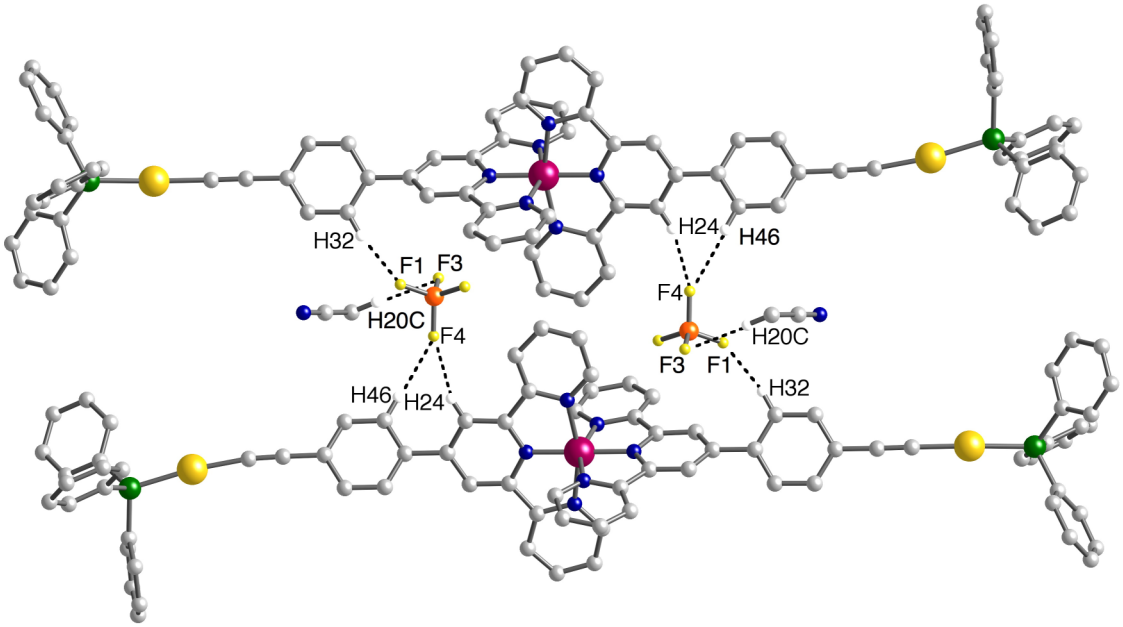

Figure S43. Representation of the crystal structure of $[Co(TpylC_6H_4C{\equiv}CAuPPh_3)_2](BF_4)_2{\cdot}(MeCN)_4$ showing the weak C–H···F–B bonds between the BF_4^- anions and the $[Co(TpylC_6H_4C{\equiv}CAuPPh_3)_2]^{2+}$ cations and MeCN molecules.

Table S1. C–H···F bond distances (Å) and angles (deg).

D-H···A	d(D-H)	d(H···A)	d(D···A)	< (DHA)°
C(32)-H(32)...F(1)	0.95	2.38	3.304(6)	164.3
C(203)-H(20C)...F(3)	0.98	2.40	3.378(8)	176.5
C(24)-H(24)...F(4)#1	0.95	2.41	3.195(6)	140.0
C(46)-H(46)...F(4)#1	0.95	2.54	3.423(6)	153.9

Symmetry transformations used to generate equivalent atoms:
#1 -x,-y+1,-z

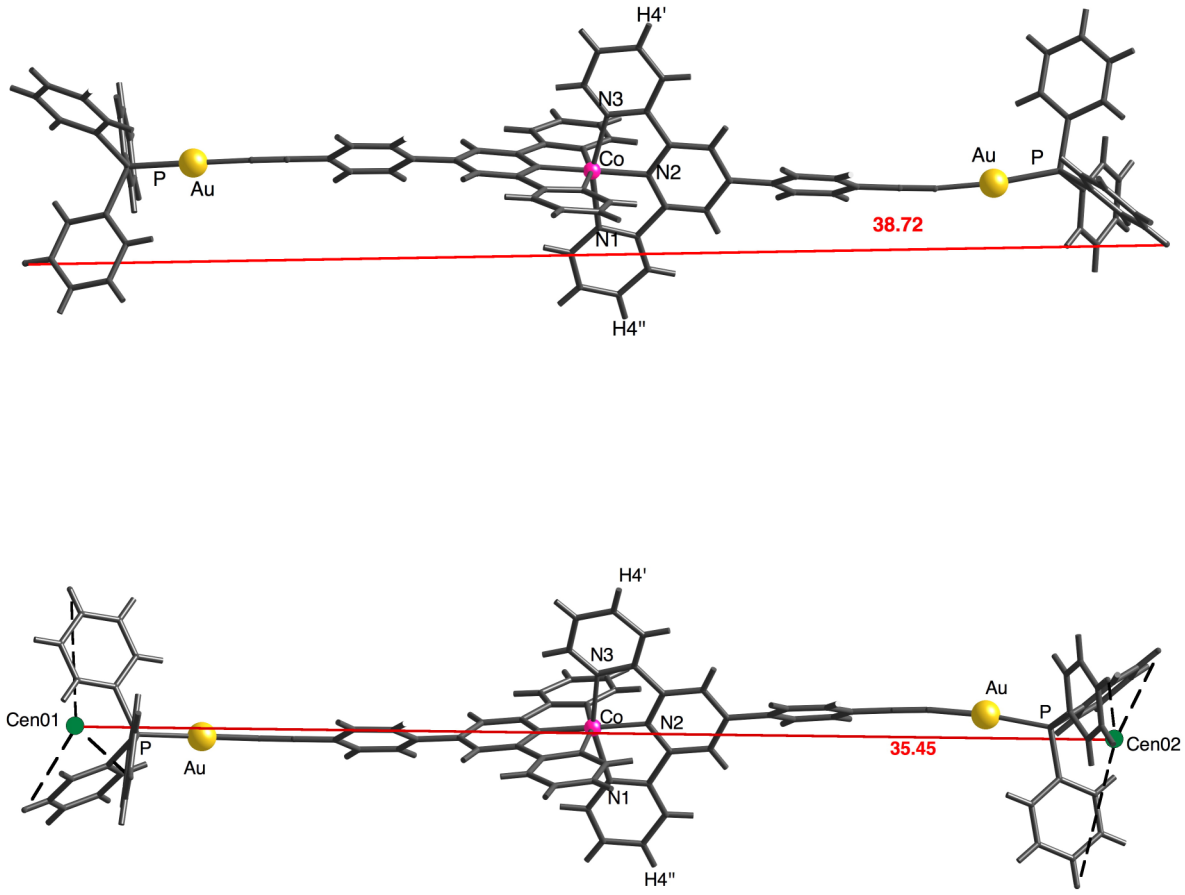

Figure S44. Representation of the crystal structure of the cation $[Co(TpylC_6H_4C{\equiv}CAuPPh_3)_2]^{2+}$ showing two significant longitudinal molecular dimensions (Å): (Up) the longest distance between a couple of oppositely-disposed phenylic hydrogens; (down) the distance between the centroids (Cen01 and Cen 02) of the three *para* hydrogens of each PPh_3 ligand.

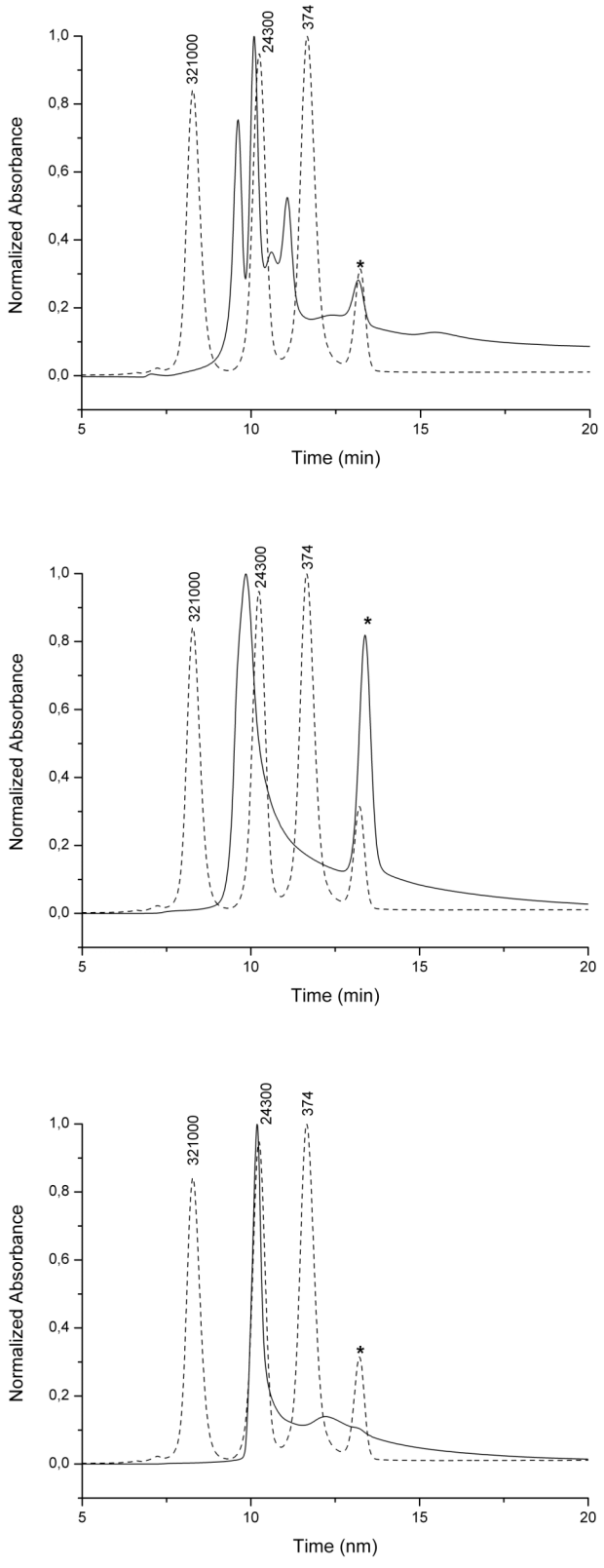

Figure S45. SEC profiles of the coordination oligomers (solid lines) $[Fe\{(TpylC_6H_4C{\equiv}C)_2Au\}]_n(ClO_4)_n$ (top), $[Co\{(TpylC_6H_4C{\equiv}C)_2Au\}]_n(BF_4)_n$ (middle) and $[Zn\{(TpylC_6H_4C{\equiv}C)_2Au\}]_n(ClO_4)_n$ (bottom), compared with a set of there monodisperse

polystyrene standards (dashed lines) measured under identical conditions. The molecular weights (in Da) of the standars are indicated in the figures. The peak marked with an asterisk corresponds to a residual impurity of the mobile phase.

The measurements were carried out using a Waters Breeze GPC system, equipped with a UV-visible detector operating at a wavelength of 272 nm. A Styragel HRE5 column covering a MW range from 2000 to 4000000 Da was used. The column was termostated at 28 ºC. HPLC-quality DMF was used as the mobile phase. The samples were dissolved in DMF at a concentration of 1.5 mg mL^{-1}. The mobile phase and sample solutions were filtered through a 0.2 μm PTFE membrane filters.